A COMPARISON OF A FERROMAGNETIC CORE COIL AND AN AIR CORE COIL AS THE SENSOR HEAD OF THE INDUCTION MAGNETOMETER

by

Hajime Ueda

B.Sc., Tohoku University, 1969

A THESIS SUBMITTED IN PARTIAL FULFILMENT OF THE REQUIREMENTS FOR THE DEGREE OF MASTER OF SCIENCE

in the Department of Geophysics and Astronomy

We accept this thesis as conforming to the required standard

The University Of British Columbia

April, 1975

In presenting this thesis in partial fulfilment of the requirements for an advanced degree at the University of British Columbia, I agree that the Library shall make it freely available for reference and study. I further agree that permission for extensive copying of this thesis for scholarly purposes may be granted by the Head of my Department or by his representatives. It is understood that copying or publication of this thesis for financial gain shall not be allowed without my written permission.

Department of Geophysics & Astronomy

The University of British Columbia
2075 Wesbrook Place
Vancouver, Canada
V6T 1W5

Date May 1st, 1975

ABSTRACT

An experimental approach is made to elucidate the input-output characteristics of a ferromagnetic core coil used as a sensor head of an induction magnetometer. Analyses made here are mainly concerned with comparison of magnetograms obtained by the permalloy core coil with respect to the one acquired simultaneously by a large open loop coil, or air core coil. Ratios of the corresponding peak-to-peak values are taken to examine distortions of the output amplitude. Blackman-Tukey's method of power spectrum estimation is applied to a portion of magnetograms, and spectral peaks are compared. The results of these analyses show that no significant distortions or harmonics are recognized in data obtained by the permalloy core coil. This suggests that the response of the permalloy core coil sensor is linear providing that the air core coil sensor is linear in response.

The demagnetization effect may be an explanation for the linear response of the permalloy core coil sensors. The demagnetization factor of the core material depends only on the geometry of the core. The permeability of the core material is suppressed in its effect if it has so large a value that its reciprocal value is much smaller than the demagnetization factor: under such circumstances, the sensitivity of the coil does not depend on the permeability of core but on the demagnetization factor. The demagnetization effect also suggests that the longer the core, the higher the coil sensitivity will be.

TABLE OF CONTENTS

LIST OF FIGURES

LIST OF TABLES

ACKNOWLEDGEMENTS

I express my appreciation and gratitude to my thesis advisor Dr. Tomiya Watanabe who directed and helped me to a great extent throughout this experiment and also encouraged me to analyze data and obtain the results which are presented in this thesis.

I gratefully acknowledge not only encouragement but also the helpful discussions and suggestions of Dr. R. D. Russell.

I appreciate also the generous help as well as the provision of the main equipment for the experiment, from Dr. B. Caner and Dr. L. Law, of the Victoria Geophysical Observatory. I thank Dr. T. Oguchi for the induction magnetometer system with permalloy core coil sensor. I also thank Mr. J. Walter for the provision of an experimental site in the University of British Columbia Research Forest.

This research received financial support from the National Research Council of Canada under grant A-3564, and from the Defence Research Board under grant 9511-112.

1. INTRODUCTION

There are many types of magnetometers used for observing the activities of the earth's magnetic field. They are the proton precession magnetometer, fluxgate magnetometer, induction magnetometer, etc. From the standpoint of aeronomy, requirements for these observation systems are such that they should cover the frequency band from 4Hz to 0.002Hz and should take the signal level from the order of milligamma to gamma or ten gammmas. The induction magnetometer turns out to be a type of instrument which satisfies these two conditions. It consists of a coil with many windings as a sensor followed by a low noise amplifier. Output signals are time derivatives of fluctuations of the magnetic field of the earth.

An open loop coil, or air core coil, has a large diameter to gain as much effective area as possible so that it can save a great number of windings. On the other hand, some high magnetic permeability materials are used as a core of the sensor coil to reduce its size and weight.

It is generally believed that magnetic devices using a ferromagnetic material for a sensor are not free from nonlinearity in response due to hysteresis, eddy current loss, Barkhausen noise of the ferromagnetic material, etc. In spite of these speculations, many magnetic stations are using a coil wound on a core which has extremely high magnetic permeability. The materials commonly used for these sensors are mumetal, permalloy, supermalloy, etc. As analysis of output wave forms, their spectra, amplitude attenuation as well as phase relative to other stations are all fundamental and important part of

research on geomagnetic micropulsations, it cannot be allowed that the sensor head introduces nonlinearity at the beginning.

It is of interest to the author of this thesis to investigate the distortions due to the nonlinearity of ferromagnetic core sensor through the analysis on magnetogram data. The approach made here is to simultaneously operate magnetometers using different kinds of sensors for actual observation and to compare the output from the different systems. Ratios of the peak-to-peak values in the output of the ferromagnetic core coil system relative to the corresponding peak-to-peak values by the air core coil system were analyzed. Also power spectra are compared between different systems.

2. CHARACTERISTICS OF A FERROMAGNETIC CORE COIL

There are many factors which should be considered if the ferromagnetic core acts as a nonlinear response element in a sensor configuration of a magnetometer. A list given in the section 2.1 shows the effects which are possible sources of nonlinear response. On the other hand, one of the probable source of nonlinear response, demagnetization effect, may result in a main factor which dominates the coil response. In that case, the response becomes linear. It requires a condition which is discussed in the section 2.2. Hysteresis response is discussed in the section 2.3. It is shown that the response due to hysteresis produces odd number harmonics.

2.1. NONLINEAR RESPONSE OF FERROMAGNETIC MATERIAL

Many possible problems with a ferromagnetic core coil have been speculated and discussed. Campbell (1967) lists the following;

1) Effective permeability varies depending upon the position of coil windings because magnetic flux leaks through the side wall of the core.

2) Magnetization caused by the primary magnetic field produces a secondary magnetic field which is, in most cases, opposite in direction to the original one. This is referred to as 'demagnetization effect'.

3) Some loss may be caused by eddy currents.

4) Barkhausen noise may be caused by microscopic magnetization of elements which form the core material.

5) Permeability of a ferromagnetic material is unstable against

thermal stress as well as mechanical shocks.

6) 'B-H' curve is a hysteresis response.

7) Some loss may be caused by completing the hysteresis loop.

8) Operation in a large bias such as the magnetic field of the earth produces second harmonics and also causes variation of the permeability.

9) Cross modulation may happen in case of two or more signals applied at the same time because of the nonlinear response of the 'B-H' curve.

The items 3, 4, 7, 8 and 9 are the ones which need discussion in terms of frequency. The problems 6, 7, 8 and 9 are the ones which originally stem from characteristics of hysteresis. Above all, the demagnetization effect plays an important role in later discussion.

2.2. DEMAGNETIZATION EFFECT

When a ferromagnetic body is placed in an ambient magnetic field, it becomes magnetized. Further, this magnetization produces secondary magnetic field whose direction is, in the case of a straight rod, opposite to the magnetization so that it tends to reduce the applied magnetic field. This secondary magnetic field is called 'demagnetization field'. The solution of Laplace's equation describes the magnetization of a body of homogeneous material placed in a uniform and parallel magnetic field, but it is difficult to calculate exactly the strength of the magnetization except for a few simple cases. An ellipsoid is one such case. Stratton (1941) obtained the magnetic potential through Laplace's equation.

The Laplace's equation becomes in ellipsoidal coordinates

$$(\eta-\zeta)R_\xi\frac{\partial}{\partial\xi}\left(R_\xi\frac{\partial\phi}{\partial\xi}\right)+(\zeta-\xi)R_\eta\frac{\partial}{\partial\eta}\left(R_\eta\frac{\partial\phi}{\partial\eta}\right)$$
$$+(\xi-\eta)R_\zeta\frac{\partial}{\partial\zeta}\left(R_\zeta\frac{\partial\phi}{\partial\zeta}\right)=0 \qquad (2.2\text{-}1)$$

where

$$R_S=\{(S-a^2)(S-b^2)(S-c^2)\}^{\frac{1}{2}} \qquad (2.2\text{-}2)$$

where a, b and c are semiprincipal axes of ellipsoid along x, y and z coordinates respectively. If the primary field is directed along the x-coordinate axis which is parallel to the major axis, a, of the ellipsoid, the potential of the applied magnetic field is

$$\phi_0=-xH_0=-H_0\left\{\frac{(\xi+a^2)(\eta+a^2)(\zeta+a^2)}{(b^2-a^2)(c^2-a^2)}\right\}^{\frac{1}{2}} \qquad (2.2\text{-}3)$$

This is also a solution of 2.2-1, and can be rewritten such as

$$\phi_0=C_1F_1(\xi)F_2(\eta)F_3(\zeta) \qquad (2.2\text{-}4)$$

where

$$C_1=-E_0\{(b^2-a^2)(c^2-a^2)\}^{-\frac{1}{2}} \qquad (2.2\text{-}5)$$

The induced potential is expected to have the form such as

$$\phi_1=C_2G_1(\xi)F_2(\eta)F_3(\zeta) \qquad (2.2\text{-}6)$$

This is substituted into 2.2-1, and

$$R_\xi\frac{d}{d\xi}\left(R_\xi\frac{dG_1}{d\xi}\right)-\left(\frac{b^2+c^2}{4}+\frac{\xi}{2}\right)G_1=0 \qquad (2.2\text{-}7)$$

Knowing $F_1(\xi)=\sqrt{\xi+a^2}$ is a solution of 2.2-7, we get an independent solution,

$$G_1(\xi)=F_1(\xi)\int\frac{d\xi}{F_1^2(\xi)R_\xi} \qquad (2.2\text{-}8)$$

Then the potential of induced magnetization becomes

$$\phi_1 = \phi_0 C_2 \int_{\xi}^{\infty} \frac{d\xi}{(\xi+a^2)R_\xi} \tag{2.2-9}$$

where C2 is an undetermined constant. Outside the ellipsoid, therefore,

$$\phi_+ = \phi_0 + \phi_1 = F_1 F_2 F_3 \left\{ C_1 + C_2 \int_{\xi}^{\infty} \frac{ds}{(s+a^2)R_s} \right\} \tag{2.2-10}$$

As $G_1(\xi)$ goes infinite at $\xi=-c^2$, the potential within the body has the form,

$$\phi_- = C_3 F_1(\xi) F_2(\eta) F_3(\zeta) \tag{2.2-11}$$

The boundary conditions determine C2 and C3. These are

$$\phi_+ = \phi_-, \quad \mu_0 \left[\frac{1}{h_1} \frac{\partial \phi_+}{\partial \xi} \right]_{\xi=0} = \mu \left[\frac{1}{h_1} \frac{\partial \phi_-}{\partial \xi} \right]_{\xi=0} \tag{2.2-12}$$

where metrical coefficient,

$$h_1 = \frac{1}{2} \left\{ \frac{(\xi-\eta)(\xi-\zeta)}{(\xi+a^2)(\xi+b^2)(\xi+c^2)} \right\}^{\frac{1}{2}}$$

μ_0 is the permeability of ambient material and μ is that of ellipsoidal body. The first of these leads to

$$C_3 = C_1 + C_2 \int_{0}^{\infty} \frac{ds}{(s+a^2)R_s} \tag{2.2-13}$$

The second one gives

$$C_2 = \frac{abc}{2} \frac{\mu_0 - \mu}{\mu_0} C_3 \tag{2.2-14}$$

With 2.2-3, the potential at any interior point of the ellipsoid is

$$\phi_- = -\frac{H_0}{1 + \frac{abc}{2\mu_0}(\mu-\mu_0)A}, \quad A = \int_{0}^{\infty} \frac{ds}{(s+a^2)R_s} \tag{2.2-15}$$

The field intensity becomes

$$H_- = -\frac{\partial \phi}{\partial x} = \frac{H_0}{1 + \frac{abc}{2\mu_0}(\mu-\mu_0)A} \tag{2.2-16}$$

Consequently, the flux density inside the ellipsoid becomes

$$B=\mu H_{-}=\frac{H_0}{\frac{1}{\mu}+\frac{abc}{2\mu_0}\left(1-\frac{\mu_0}{\mu}\right)A} \qquad (2.2\text{-}17)$$

if $\mu >> \mu_0$.

$$B=\frac{H_0}{\frac{1}{\mu}+Nd}, \quad Nd=\frac{abc}{2\mu_0}A \qquad (2.2\text{-}18)$$

from this equation, it is clear that when is very large, the effective permeability B/Ho reduces to a value of 1/Nd. Thus the permability is determined by the geometrical constant only. Therefore, in this case, overall response of a ferromagnetic core coil is free from its nonlinear hysteresis response.

In the case of magnetization of a slim elliptic cylinder along its length, demagnetization factor Nd is calculated by Osborn (1945).

$$Nd=\frac{1}{m^2-1}\left\{\frac{m}{\sqrt{m^2-1}}\ln\left(m-\sqrt{m^2-1}\right)-1\right\} \qquad (2.2\text{-}19)$$

where m is a ratio of its length to the cross-sectional diameter. If m >>1,

$$Nd=\frac{1}{m^2}\{\ln 2m-1\} \qquad (2.2\text{-}20)$$

Table 2.1 shows the demagnetization factor for a rod, a prolate ellipsoid and an oblate ellipsoid. Data for the rod given here is obtained through the experiment by Bozorth (1951).

For a given core diameter, the longer the core length the higher is the sensitivity of the sensor, because equation 2.2-18 shows that the reciprocal value of magnetization, or the effective permeability in this case, is almost prcpcrtional to the square of the length. Fig. 2.1 for a rod shows clearly that, for a longer core, higher permeability is required to

Dimensional Ratio (length/diameter)	Rod	Prolate Ellipsoid	Oblate Ellipsoid
0	1.0	1.0	1.0
1	.27	.3333	.3333
2	.14	.1735	.2364
5	.040	.0558	.1248
10	.0172	.0203	.0696
20	.00617	.00675	.0369
50	.00129	.00144	.01472
100	.00036	.000430	.00776
200	.000090	.000125	.00390
500	.000014	.0000236	.001567
1000	.0000036	.0000066	.000784
2000	.0000009	.0000019	.000392

Table 2.1. Demagnetization factors of rod and ellipscids magnetized parallel to the long axis (Bozorth, 1951).

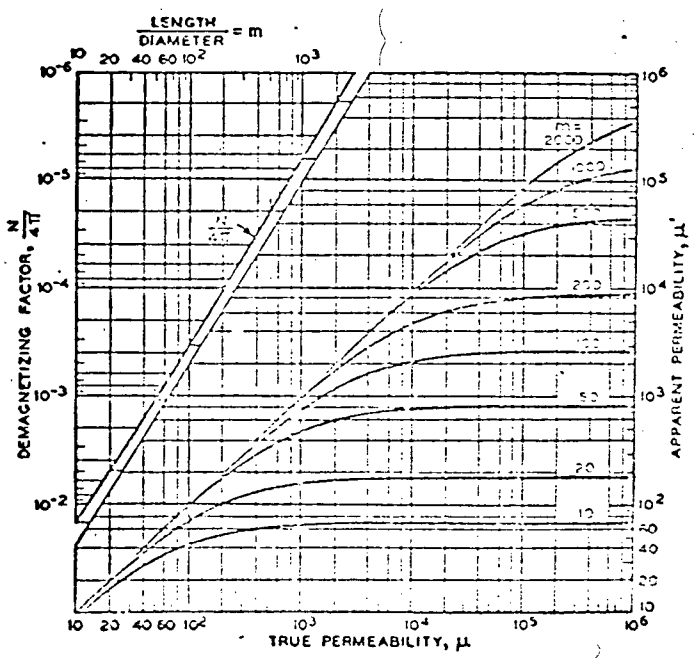

Fig. 2.1. Chart for converting true to apparent permeability of ferromagnetic cylinders of given ratio of length to diameter (Bozorth, 1951).

secure the linear region in which the demagnetization effect dominates overall response. Considering sufficiently high permeability values attainable for some ferromagnetic materials, there seems to be no difficulty in suppressing nonlinear response inherent in the original magnetic permeability.

2.3. HYSTERESIS RESPONSE

If the 'B-H' relation dominates coil response rather than the linear response by virtue of the demagnetization effect, some harmonics of the alternating primary field are expected to result from the hysteresis of the ferromagnetic material. Peterson (1928) carried out a mathematical analysis of the hysteresis response.

It is assumed that the applied magnetic field is purely sinusoidal and its intensity is not strong enough to cause eddy current loss. When H is the maximum amplitude, the magnetic field, h, becomes

$$h = H \cos \omega t \qquad (2.3\text{-}1)$$

For one cycle of this excitation, each hysteresis curve is assumed to be one complete loop, and the flux density B, is a function of the applied field h, its maximum value H, and the sign of dh/dt.

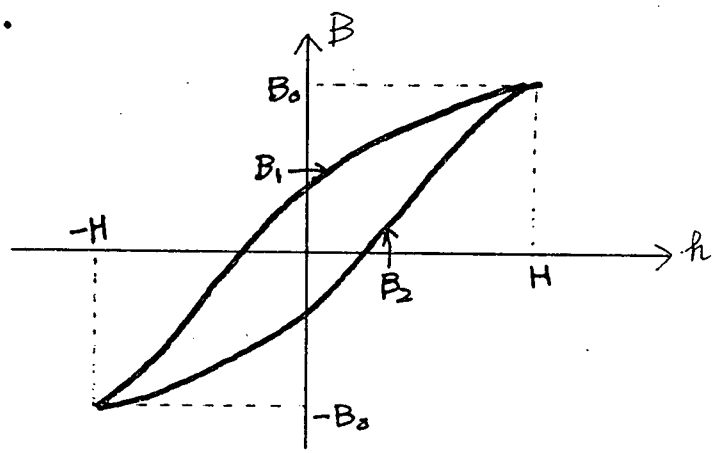

The sign of dh/dt splits the hysteresis loop into two branches, top and bottom ones; B1 and B2, respectively. Each branch is expressed by the same form

$$B(h,H)=\sum_{m=0}^{\infty}\sum_{n=0}^{\infty} a_{mn} h^m H^n \tag{2.3-2}$$

where

$$a_{mn}=\frac{1}{m!\,n!}\left.\frac{\partial^{m+n}B}{\partial h^m \partial H^n}\right|_{h=0,\,H=0} \tag{2.3-3}$$

As B=0, at h=0 and H=0,

$$a_{00}=0 \tag{2.3-4}$$

The hysteresis loop is symmetric about the origin, and its each branch has the relation,

$$B_1(h,H)=-B_2(-h,H) \tag{2.3-5}$$

Then,

$$\begin{aligned} B_1(h,H)=\; & a_{10}h+a_{01}H \\ & +a_{20}h^2+a_{11}hH+a_{02}H^2 \\ & +a_{30}h^3+a_{21}h^2H+a_{12}hH^2+a_{03}H^3+\cdots \end{aligned} \tag{2.3-6}$$

$$\begin{aligned} B_2(h,H)=\; & a_{10}h-a_{01}H \\ & -a_{20}h^2+a_{11}hH-a_{02}H^2 \\ & +a_{30}h^3-a_{21}h^2H+a_{12}hH^2-a_{03}H^3+\cdots \end{aligned} \tag{2.3-7}$$

These branches meet at the loop tip,

$$B_1(H,H)=B_2(H,H) \tag{2.3-8}$$

Substituting 2.3-6 and -7 into -8, we obtain a relation up to third order of H.

$$a_{01}H+(a_{20}+a_{02})H^2+(a_{21}+a_{03})H^3=0 \tag{2.3-9}$$

Since this relation holds for any value of H,

$$a_{01}=0,\quad a_{12}=-a_{20},\quad a_{03}=-a_{21} \tag{2.3-10}$$

2.3-6 and -7 become

$$B_1(h,H) = a_{10}h - a_{02}h^2 + a_{11}hH + a_{02}H^2 + a_{30}h^3 - a_{03}h^2H + a_{12}hH^2 + a_{03}H^3 \tag{2.3-11}$$

$$B_2(h,H) = a_{10}h + a_{02}h^2 + a_{11}hH - a_{02}H^2 + a_{30}h^3 + a_{03}h^2H + a_{12}hH^2 - a_{03}H^3 \tag{2.3-12}$$

Let

$$\alpha = a_{02}H^2 + a_{03}H^3 = B(0,H)$$

$$\beta = (a_{10} + a_{11}H) + a_{12}H^2$$

$$\gamma = a_{30}H^3 \tag{2.3-13}$$

Then,

$$B_1(H\cos\omega t, H) = \alpha + \beta\cos\omega t - \alpha\cos^2\omega t + \gamma\cos^3\omega t \tag{2.3-14}$$

$$B_2(H\cos\omega t, H) = -\alpha + \beta\cos\omega t + \alpha\cos^2\omega t + \delta\cos^3\omega t \tag{2.3-15}$$

From these two equations we see that α represents the remanence and β an approximate permeability.

Letting

$$A = \frac{\alpha}{2}, \quad B = \beta + \frac{3}{4}\delta, \quad C = -A, \quad D = \frac{\delta}{4} \tag{2.3-16}$$

the equations 2.3-14 and 2.3-15 can be modified further,

$$B_1(H\cos\omega t, H) = A + B\cos\omega t + C\cos 2\omega t + D\cos 3\omega t \tag{2.3-17}$$

$$B_2(H\cos\omega t, H) = -A + B\cos\omega t - C\cos 2\omega t + D\cos 3\omega t \tag{2.3-18}$$

Both branches of hysteresis curve are combined in the form,

$$B = \frac{b_0}{2} + \sum_{k=1}^{\infty}(b_k\cos k\omega t + a_k\sin k\omega t) \tag{2.3-19}$$

where

$$a_k = \frac{1}{\pi}\left\{\int_{\pi}^{0} B_2(A,H)\sin\omega t\, d\omega t + \int_{0}^{\pi} B_1(A,H)\cos\omega t\, d\omega t\right\}$$

$$= \frac{1}{\pi}\int_{0}^{\pi}\{B_1(A,H)[1+(-1)^{k+1}]\}\sin k\omega t\, d\omega t$$

(2.3-20)

$$b_k = \frac{1}{\pi}\int_{0}^{\pi}\{B(A,H)[1+(-1)^{k+1}]\}\cos k\omega t\, d\omega t$$

(2.3-21)

so that

$$a_k = \frac{2}{\pi}\int_{0}^{\pi}(A + C\cos^2\omega t)\sin k\omega t\, d\omega t$$

(2.3-22)

$$b_k = \frac{2}{\pi}\int_{0}^{\pi}(B\cos\omega t + D\cos 3\omega t)\cos k\omega t\, d\omega t$$

(2.3-23)

The coefficients

$$a_0, a_2, a_4, \cdots\cdots, a_{2n}, \cdots\cdots$$

$$b_0, b_2, b_4, \cdots\cdots, b_{2n}, \cdots\cdots$$

all become zero, because of the symmetry of the loop. The fundamental and the third harmonic components have ccefficients,

$$a_1 = \frac{4}{\pi}\left(A - \frac{C}{3}\right) = \frac{8}{3\pi}(a_{02}H^2 + a_{03}H^3) \quad (2.3\text{-}24)$$

$$b_1 = a_{10}H + a_{11}H^2 + \left(a_{12} + \frac{3}{4}a_{30}\right)H^3 \quad (2.3\text{-}25)$$

$$a_3 = \frac{4}{\pi}\left(\frac{A}{3} + \frac{3}{5}C\right) = -\frac{8}{15\pi}(a_{02}H^2 + a_{03}H^3) \quad (2.3\text{-}26)$$

$$b_3 = D = \frac{1}{4}a_{30}H^3 \quad (2.3\text{-}27)$$

The voltage across the output terminals is

$$E = 10^{-8} NA \frac{dB}{dt} \qquad (2.3\text{-}28)$$

where N is the number of turns of the winding, A is the cross-sectional area.

$$E = 10^{-8} NA(\omega a_1 \cos\omega t + 3\omega t a_3 \cos 3\omega t - \omega b_1 \sin\omega t - 3\omega t b_3 \sin 3\omega t) \qquad (2.3\text{-}29)$$

Therefore it is more likely that the third harmonic rather than the second harmonic signal will be produced by the hysteresis response.

3. EXPERIMENT

3.1. INSTRUMENTATION

Three induction magnetometers have been operated at the University of British Columbia Research Forest, Maple Ridge, British Columbia since September 10, 1973.

The setup of the experiment is schematically shown on Fig. 3.1. System A consists of an air core coil as the sensor head and a semiconductor parametric amplifier which can take as high an output impedance as the 200 k-ohm of the sensor with a noise figure less than 3db. System B uses a permalloy core coil sensor which is connected to parametric amplifier identical to that of the system A. Direct comparison is possible between the outputs from the two systems A and B. System C has a permalloy core coil with FET chopper amplifier. To obtain ncise levels as low as 0.1 micro-volt peak-to-peak, this amplifier employs intensive filtering throughout (Fig. 3.4). Outputs of these systems are recorded on a 7 channel FM magnetic tape recorder together with the output of a fluxgate magnetometer, clock pulses and a reference FM carrier signal. Sensitivity of this recorder is adjusted to be 2 volts per 40% frequency deviation of FM carrier signal. This FM recorder determines the dynamic range of systems and it is 40db in rms base.

Coil constants are given in Table 3.1. The air core coil was constructed and calibrated by B. Caner (1970). Data of the ferromagnetic core coil are obtained by T. Watanabe from the frequency response of the coil. The signal from the oscillator is introduced to the coil through a resistor which has a value

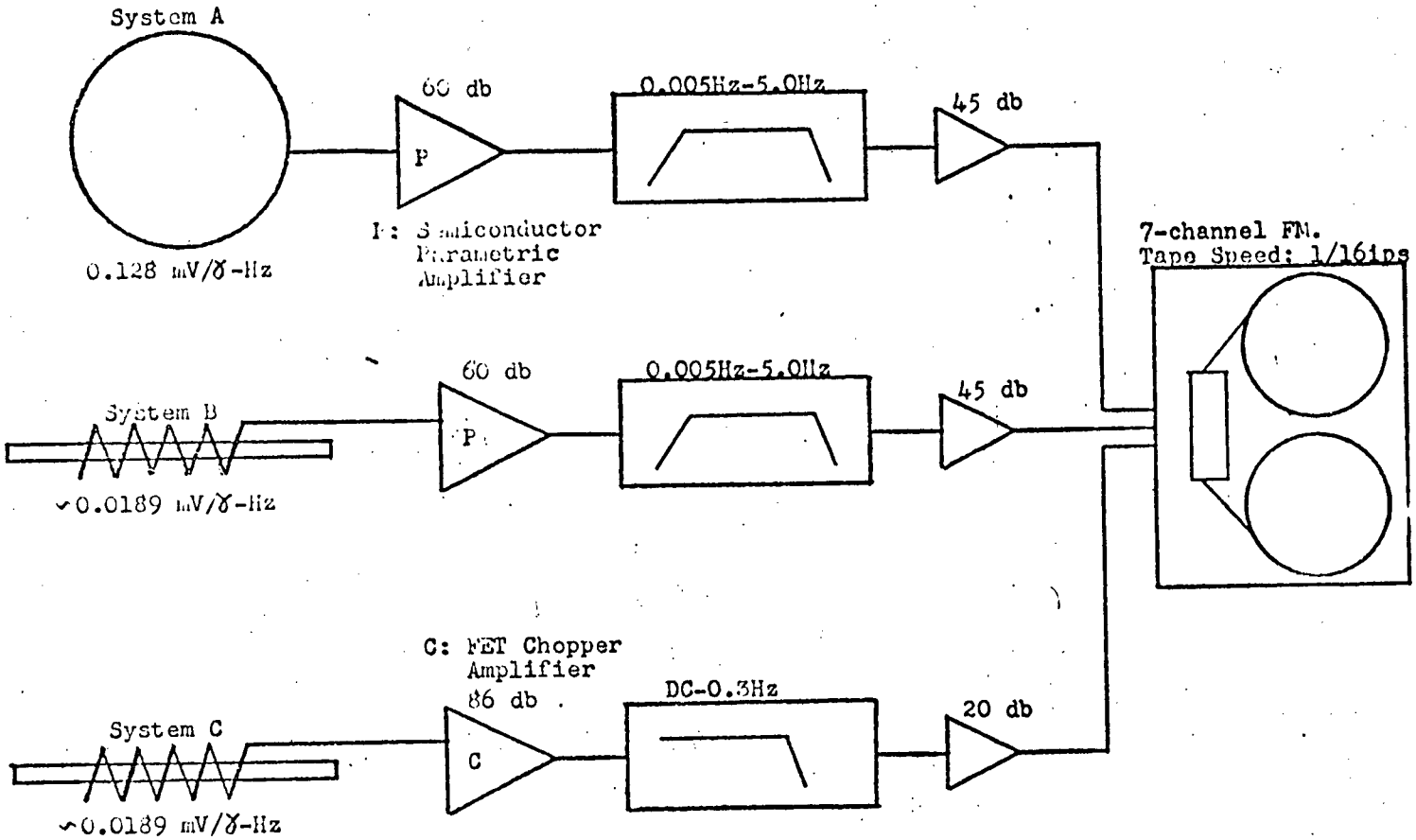

Fig. 3.1. Schematic diagram of experimental setup.

	Air core coil	Permalloy core coil
Weight	175 kg	12 kg
Dimension	Diameter; 1.27 m	Core length; 1.0 m Cross-section; 2.0x2.0 cm
Number of turns	16,000 turns	50,000 turns
DC resistance	5.45 k-ohm	158 ohm
Resonance frequency	84 Hz	400 Hz
Self inductance	530 H	170 H
Stray capacitance	6.7 nF	0.8 nF
Damping resistor	200 k-ohm	10 k-ohm
Johnson noise (DC - 4Hz)	18.5 nV(RMS)	3.17 nV(RMS)
Sensitivity	0.128 mV/ -Hz	0.0189 mV/ -Hz

Table 3.1. Coil characteristics

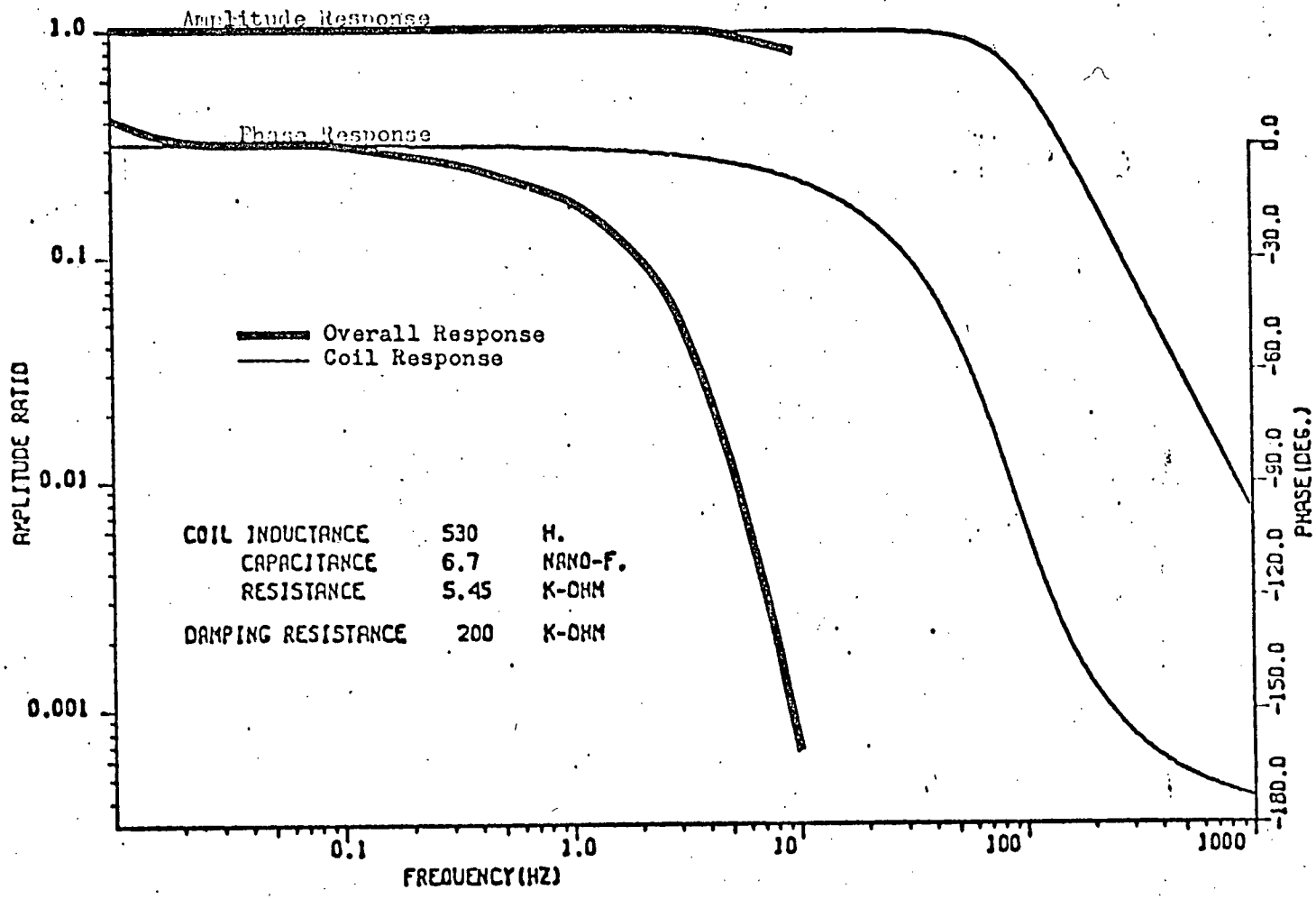

Fig. 3.2. Attenuation and phase response of system A. Coil response includes the input impedance of the preamplifier.

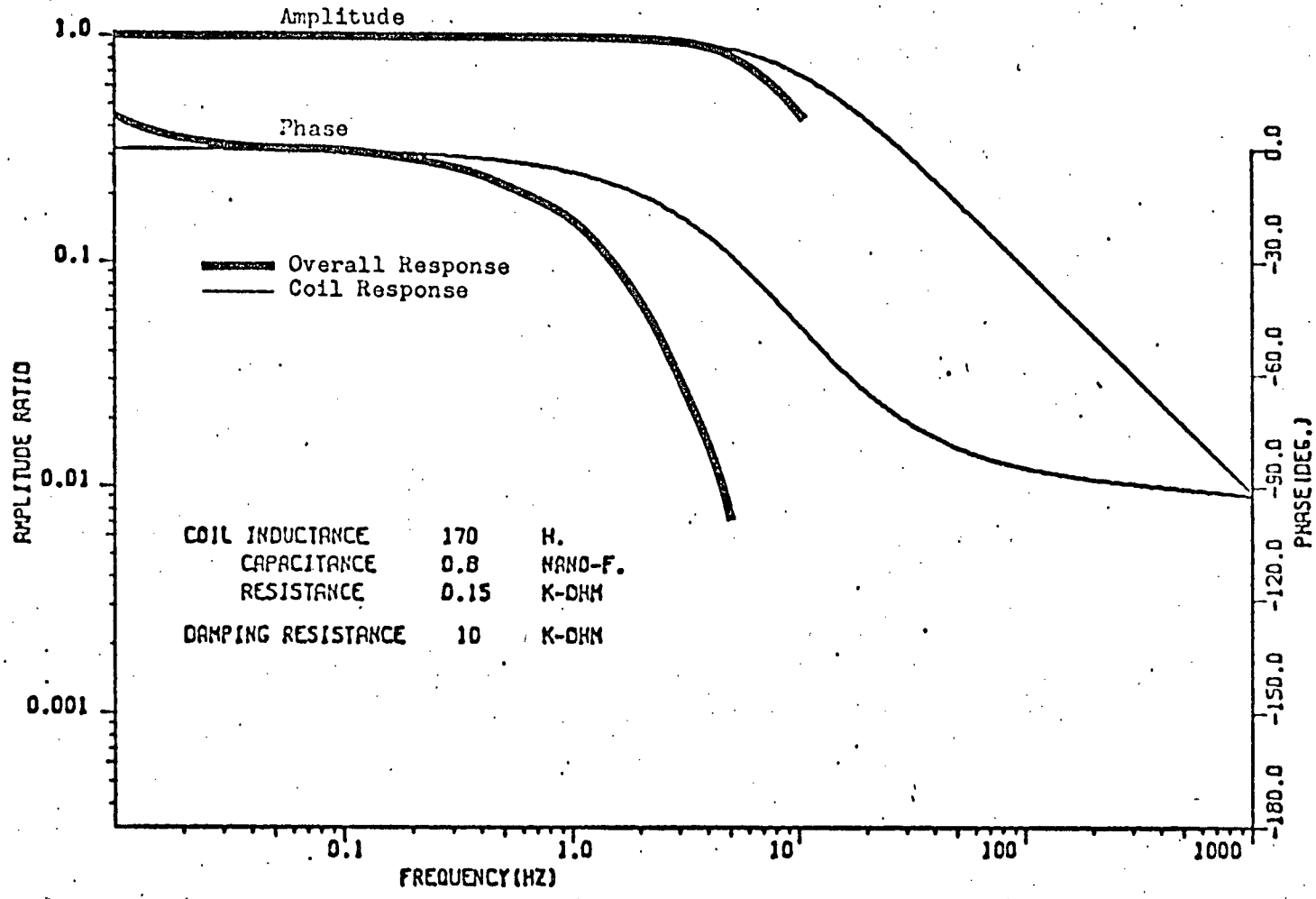

Fig. 3.3. Attenuation and phase response of system B. Coil response includes the input impedance of the preamplifier.

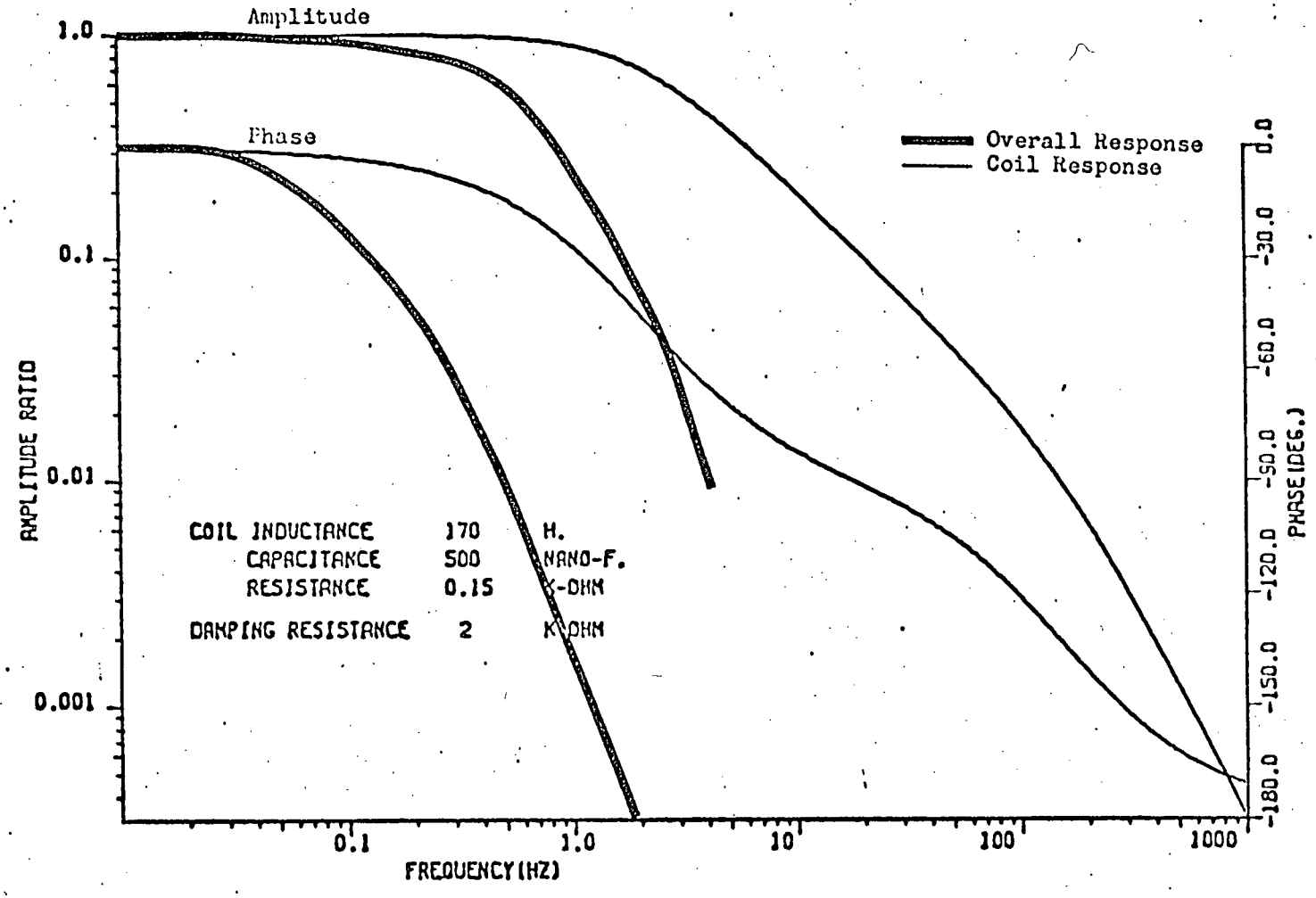

Fig. 3.4. Attenuation and phase response of system C. Coil response includes the input impedance of the preamplifier.

much smaller than the resistance of the coil windings. Then the current through this resistor is measured as a function of frequency. The frequency response of the coil is sensitive to the input impedance of the preamplifier. The combined response of coil and amplifier impedance is shown together with the overall system response for each sensor coils on Fig. 3.2, 3.3 and 3.4.

3.2 SOME CONSIDERATIONS ON COIL CHARACTERISTICS

The sensor coil is approximated to be an N turn winding whose radius is constant. Corresponding to the uniformly varying magnetic field, the voltage induced in the coil, Eo, is

$$E_o = -\frac{d\Phi}{dt} = -\frac{d}{dt}\{NS\mu h\} \qquad (3.2\text{-}1)$$

where S is the cross-sectional area of the coil, μ is permeability of the coil core, and h is the magnetic field component perpendicular to the coil cross-section. Usually, permeability is measured as a normalized value to the vacuum one, so that

$$E_o = 4\pi \cdot 10^{-7} \bar{\mu}_e N S \dot{h} \qquad (3.2\text{-}2)$$

According to data for the air core coil in Table 3.1, N=16,000, S=1.28 m² and $\bar{\mu}_e = 1$. The magnetic field, h, is measured conventionally in milligammas which is equal to $1/4\pi \times 10^{-5}$ AT/m in MKS units. The sensitivity of air core coil becomes

$$E_o = 0.128\ \mu V/m\gamma\text{-}Hz \qquad (3.2\text{-}3)$$

As the total gain of the amplifier is calibrated to 1.87×10^5, a magnetic field variation of 1 milligamma peak gives rise to a deflection of 23.5 mV on the recorders.

Campbell (1960) suggested a simple form of equivalent

circuit to approximate characteristics of sensor coil.

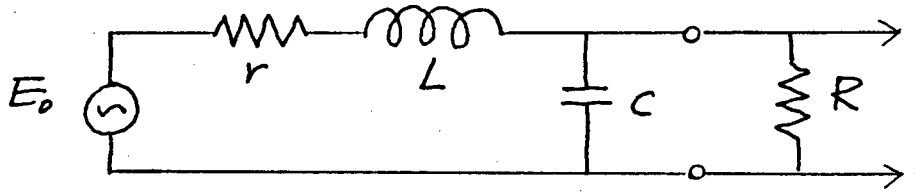

Where r is the resistance of windings, C is the stray capacitance, L is the self-inductance. R is an optional resistor which is shunting the output terminals of coil. This resistor damps the resonance peak of coil and, with minimal effort, provides maximal flat amplitude response. The transfer function of the above equivalent circuit is

$$H(\omega)=\frac{R}{r+R-\omega^2LCR+j\omega(L+rR)} \tag{3.2-4}$$

So the amplitude response is

$$A(\omega)=|H(\omega)|=R/N(\omega) \tag{3.2-5}$$

where

$$N(\omega)=\{[r+R)-\omega^2LCR]^2+\omega^2(L+rCR)^2\}^{\frac{1}{2}} \tag{3.2-6}$$

It is desirable that there be no irregular peaks in the amplitude response,

$$A(\omega)\leq\frac{R}{r+R} \tag{3.2-7}$$

for all ω. That is,

$$R\leq\{L^2/(2LC-r^2C^2)\}^{\frac{1}{2}} \tag{3.2-8}$$

where 2L > rC, which most sensors with many windings satisfy. On the other hand, for a coil wound with extremely thin, or highly resistive wire and with small inductance, the loss by the resistive component becomes so large that no resonance peaks appear higher than the level at DC. The maximum limit value of R also satisfies the condition that the first and second

derivatives of N(w) be positive, for all ω. The amplitude response damped by R, therefore, decreases monotonically toward the higher frequency region.

As the damping resistor shunts the output of the coil, it produces additional thermal noise.

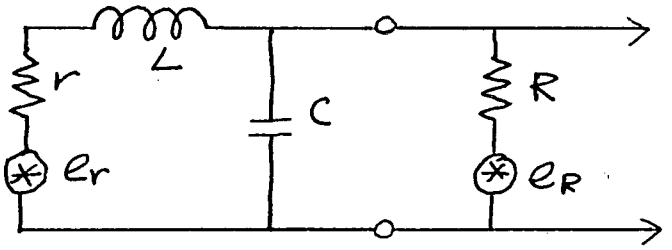

where e_r and e_R are rms value of thermal noise of resistive components, r and R, respectively. Using the current source representation, it becomes

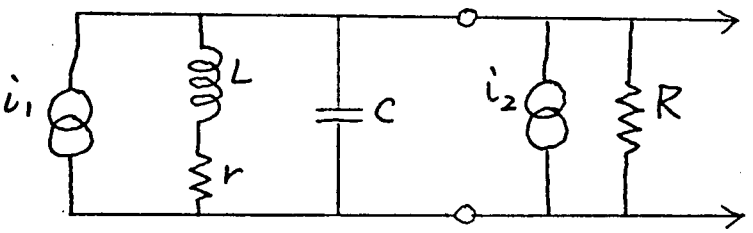

These two thermal noises are considered to be uncorrelated, and two current sources are replaced by one source such that

$$i_n = \sqrt{i_1^2 + i_2^2} = \left\{ \left(\frac{e_1}{r + j\omega L} \right)^2 + \left(\frac{e_2}{R} \right)^2 \right\}^{\frac{1}{2}} \qquad (3.2\text{-}9)$$

Similarly, a current source equivalent to the voltage induced by magnetic field variation is

$$i_s = \frac{E_0}{r + j\omega L} = \frac{4\pi \cdot 10^{-12} \mu_0 N S \dot{A}}{r + j\omega L} \qquad (3.2\text{-}10)$$

Thermal noise, then, can be estimated as an equivalent magnetic variation.

$$\dot{h}_n = \frac{r + j\omega L}{4\pi \cdot 10^{-12} \mu_0 N S} \left\{ \left(\frac{e_1}{r + j\omega L} \right)^2 + \left(\frac{e_2}{R} \right)^2 \right\}^{\frac{1}{2}} \qquad (3.2\text{-}11)$$

4. ANALYSIS

Outputs of the amplifiers were recorded on a magnetic tape by an FM slow speed analog tape recorder. The tape was then played back at a speed 15 times faster than for the recording. Then the data was digitized at a rate of 29 points per second after passing through a lowpass filter whose cutoff frequency is 8 Hz and attenuation slope 24 db/oct.

There was a period of active geomagnetic micrcpulsation on October 10, 1973. The data of a 282 sec duration starting from 21:42'06" UT were analyzed mainly because the data is free of sporadic noise inherent to the parametric amplifiers used in this experiment.

As a preliminary comparison of the three channels, least squares fits of these signals were taken. Secondly, the amplitude ratio of the permalloy core coil signal to the air core coil signal was examined and finally, power spectra of the three were compared.

4.1. LEAST SQUARES FIT

A least squares fit was tried between the air core coil signal and each of the permalloy core coil signals. Commencing on 21h 42m 06s UT, data of 2 min 21 sec duration was sampled from the record of October 10, 1973. There is a medium level of geomagnetic micropulsation activity during this period and its major frequency components lie in the range 0.02-0.08Hz.

Let Yb and Yc be the output voltage of the permalloy core coil systems, B and C, respectively. As mentioned already, the system B has a parametric amplifier immediately following the

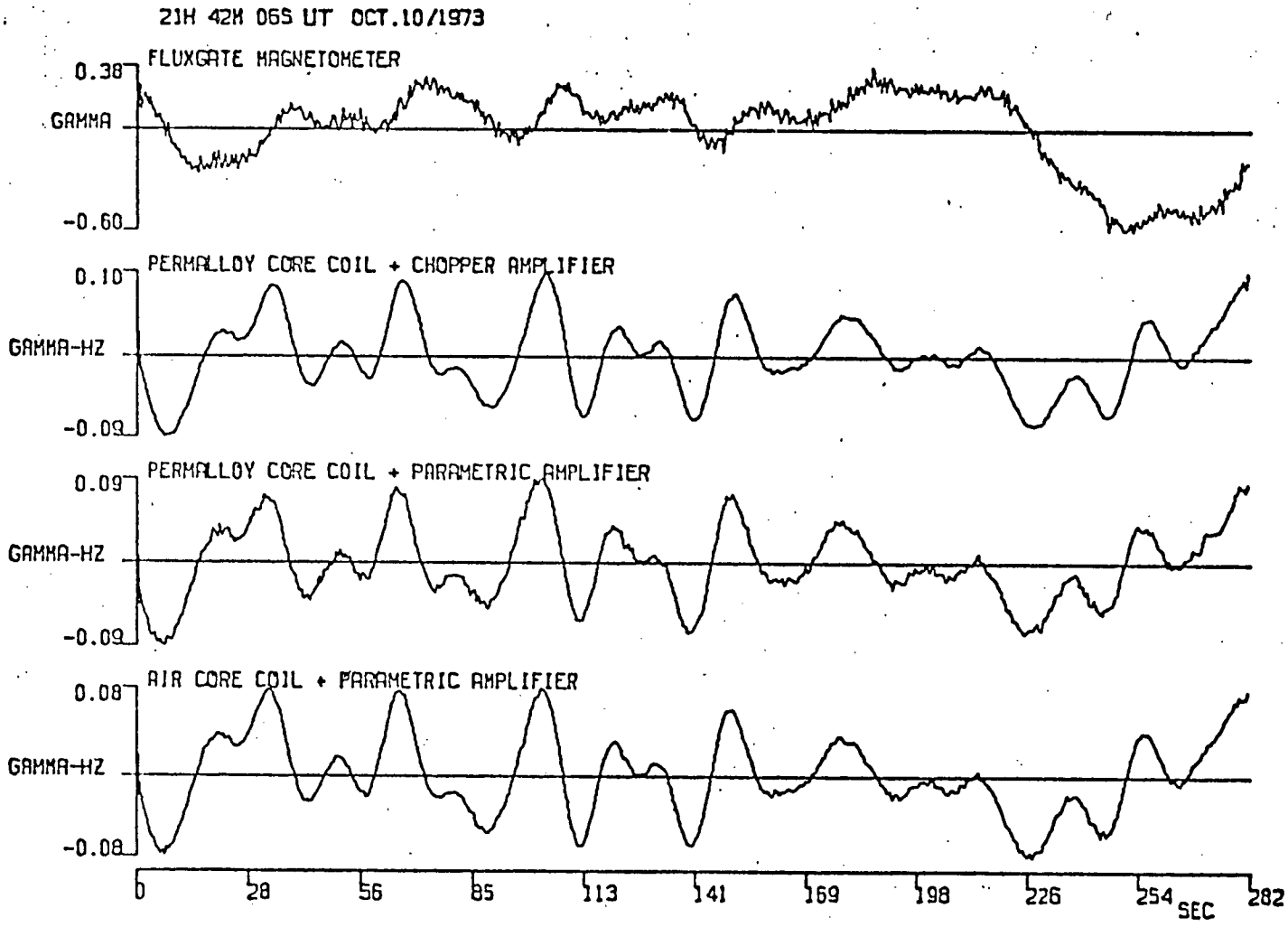

Fig. 4.1. Magnetogram of 21h 42m 06s UT on October 10, 1973.

sensor coil and the system C has a FET chopper amplifier. X is used to denote the output voltage of the air core coil system (system A). The fittng curve is given by

$$YF_\ell = \sum_{n=0} k_n X_\ell^n \qquad (4.1\text{-}1)$$

From this, the curve is fitted to Yb and Yc using the least squares fitting i.e.

$$SS = \sum (Yb_\ell - YF_\ell)^2 \qquad (4.1\text{-}2)$$

is minimized over the 141 sec duration of the record. The gain difference between channels is essentially k1. The higher order coefficients represent the possible nonlinear effects due to the ferromagnetic core as mentioned in section 2.1 already.

Although the amplitude response of the amplifiers in each systems is taken to be flat enough over the frequency content of the signal, differences in phase are not negligible. This affects the results of the least squares fit method. The characteristics of the coil response will be projected on the coefficients if these phase responses are compensated, ideally with filters which have the complementary responses to the amplifiers. Here it is done simply by realigning the relative position of the data of each channel and the smallest sum of squares is obtained. If relative lag is τ sec between records,

$$\sin \omega t \rightarrow \sin \omega(t+\tau) = \sin(\omega t + \omega\tau)$$

so that this operation is equivalent to using a phase shifter which gives a phase shift proportional to frequency. The best result is obtained when a lag of -0.55 sec is placed on the

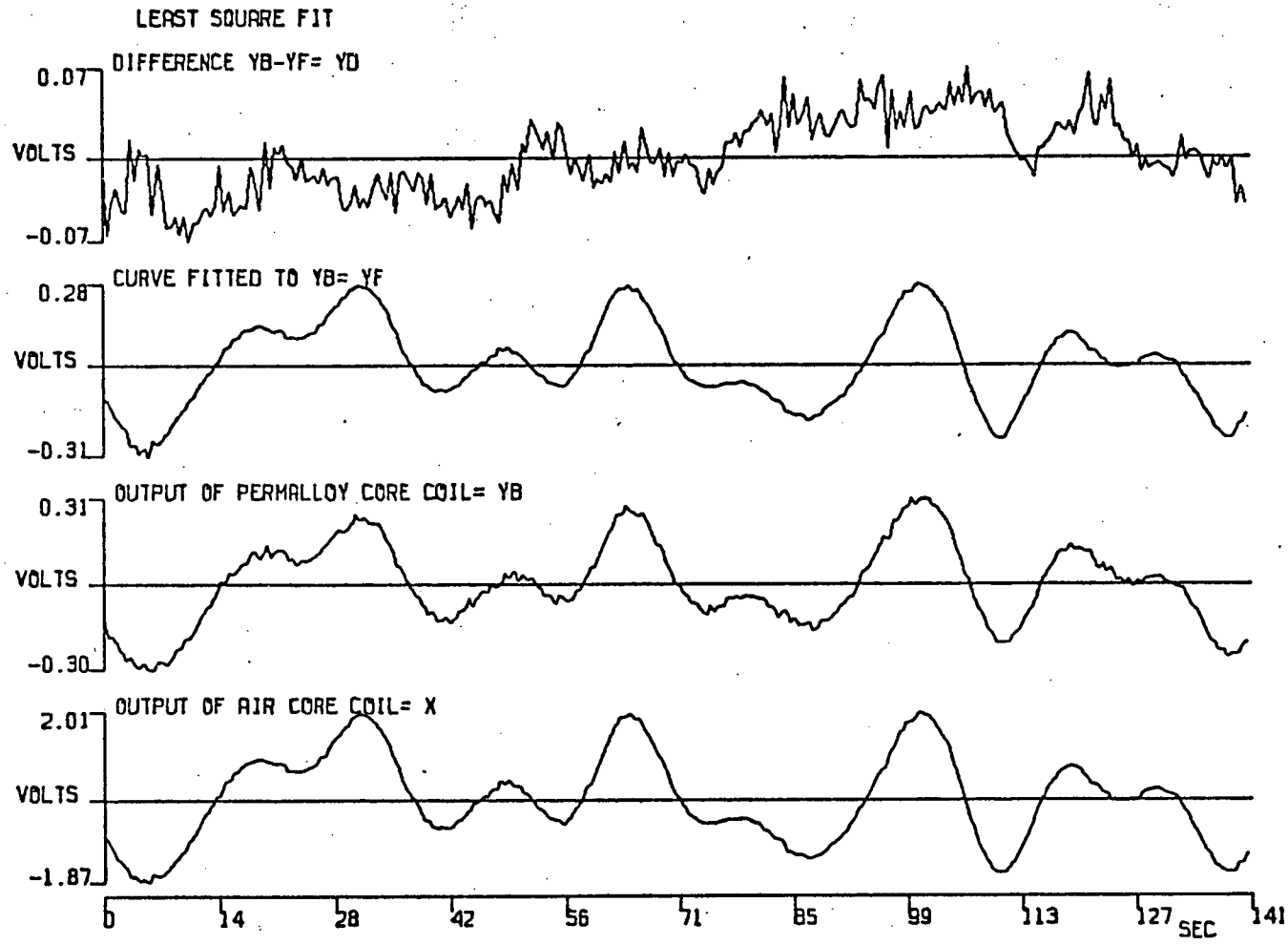

Fig. 4.2. Least squares fit. Output of system A is fitted to the one of system B.

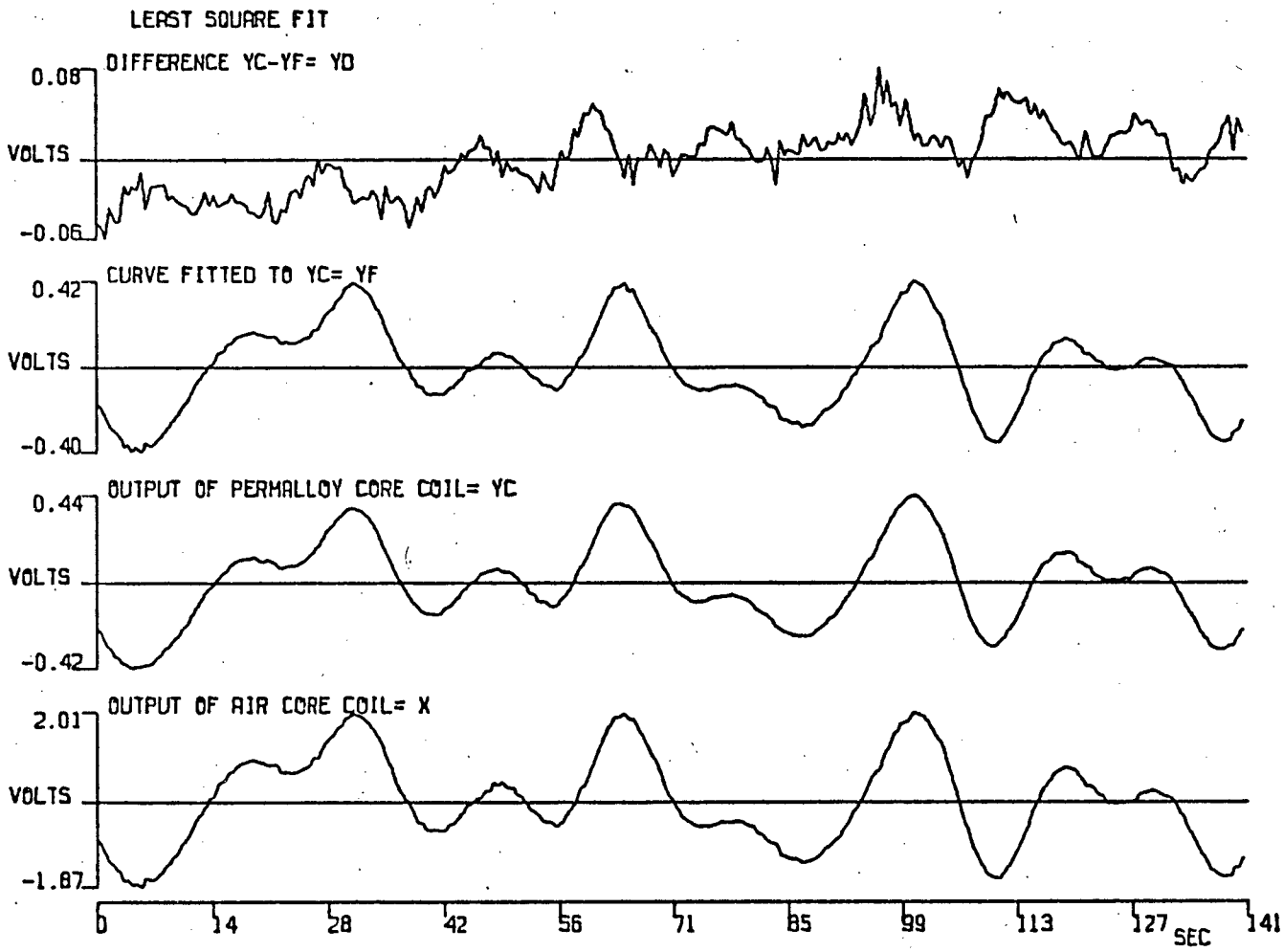

Fig. 4.3. Least squares fit. Output of system A is fitted to the one of system C.

	System B		System C	
n	Kn	Kn x 2^n	Kn	Kn x 2^n
1	0.14154	0.28308	0.18365	0.36730
2	(0.01382)	(0.05528)	(-0.00733)	(-0.02932)
3	(-0.00340)	(-0.02720)	0.01111	0.08888
4	-0.00561	-0.08976	(0.00157)	(0.02512)
5	(0.00195)	(0.06240)	(-0.00097)	(-0.03104)

Table 4.1. Coefficients of the least squares fit. Air core coil signal is fitted to permalloy core coil signal. Bracketted values are not significant.

record of system B with respect to that of the system A. This lag is equivalent to about 9.9 degrees lead for a signal of 0.05 Hz. In case of system C, it was 3.3 sec lag, which is about 59.4 degree lag for 0.05 Hz.

The results are shown on Fig. 4.2 and Fig. 4.3. As the maximum amplitude of X is 2 volts, the terms $k_n X^n$ contribute the maximum amount of $k_n 2^n$. These maximum contributions are listed together with the coefficients k_n on Table 4.1. The largest value appears for the fourth order coefficient in the fit to the signal of system B, and for the third order to the system C signal. The inconsistency of the magnitude of least squares fit coefficients between the results by system B and the one by system C may be caused by the noise of the tape recorder used in this experiment. The noise level of the FM tape recorder is 0.02 volts rms, so that noise higher than 0.06 volts occurs with probability less than 0.12 %. But such noise is still a substantial part of many values in columns 3 and 5 of Table 4.1, so that many of the coefficients are masked by tape noise.

4.2. AMPLITUDE RATIO

A straightforward comparison of the signal amplitude is made by taking the ratio of each permalloy core coil signal to the air core coil signal. It is appropriate to use peak-to-peak readings. They are free of dc offset and phase shift. Besides, they are less affected by noise because of relatively higher S/N ratios. Data commencing on 21h 42m 06s UT was taken from the disturbed day record, October 10, 1973.

To obtain peak-to-peak readings, maximum and minimum values of the signal waveform were collected. Then, difference between a succesive pairs of values was obtained which gives a peak-to-peak reading. One maximum/minimum reading is used for calculating two peak-to-peak values in the series. Consequently, they are opposite in polarity.

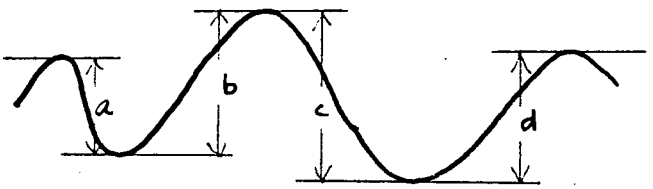

Readings of noise, mostly sporadic pulses caused by amplifiers, are then deleted.

Fig. 4.4 and Fig. 4.5 show the ratios of the readings by the permalloy core coil systems to the peak-to-peak reading of the air core coil system signal. Apparently the noise of every system affects small peak-to-peak values. Plots for smaller values are more scattered. Studies of noise characteristics as well as the probability of the ratio of two normal variables enable us to draw the distribution range of ratio values with respect to the value of the output of system A.

4.2.1. RELATIVE SENSITIVITY AND RATIO OF TWO NORMAL VARIABLES

Let n1 be the noise in a peak-to-peak reading on system A signal, Y1. Then, we have

$$y_1 = x + n_1 \qquad (4.2.1\text{-}1)$$

where x is the signal, the true peak-to-peak reading. The corresponding peak-to-peak reading on system B channel, Y2 is given by

$$y_2 = xS + n_2 \qquad (4.2.1\text{-}2)$$

where S is the gain of system B relative to system A. The ratio is

$$R=\frac{xS+n_2}{x+n_1} \qquad (4.2.1\text{-}3)$$

If x is much larger than n1,

$$R=S\left(1+\frac{n_2}{xS}\right)/\left(1+\frac{n_1}{x}\right)\simeq S\left(1+\frac{n_2}{xS}-\frac{n_1}{x}\right) \qquad (4.2.1\text{-}4)$$

so that

$$x(R-S)\simeq n_2-n_1S \qquad (4.2.1\text{-}5)$$

If noise of each channel is assumed to follow a normal distribution, the quantity x(R-S), follows approximately a normal distribution, $N(0,\sigma_1^2+(\sigma_2 S)^2)$; the average value is zero and the variance is equal to $\sigma_1^2+(\sigma_2 S)^2$ where σ_1 and σ_2 are the standard deviations of n1 and n2, respectively. Consequently, the mean value becomes

$$\langle x(R-S)\rangle\simeq 0 \qquad (4.2.1\text{-}6)$$

or

$$\langle xR\rangle\simeq\langle x\rangle S \qquad (4.2.1\text{-}7)$$

That is,

$$S=\frac{\langle xR\rangle}{\langle x\rangle}\simeq\frac{\langle y_1R\rangle}{\langle y_1\rangle} \qquad (4.2.1\text{-}8)$$

Thus, an approximate value of the relative sensitivity can be obtained. The sensitivity of system B relative to the one of system A was found to be 0.1438. For system C, it is 0.1838. Moreover, knowledge of this sensitivity makes it possible to check the assumption on the characteristics of ncise, because the quantity,

$$y_2-Sy_1=n_2-Sn_1 \qquad (4.2.1\text{-}9)$$

must follow a normal distribution, $N(0,\sigma_2^2+(\sigma_1 S)^2)$, if the

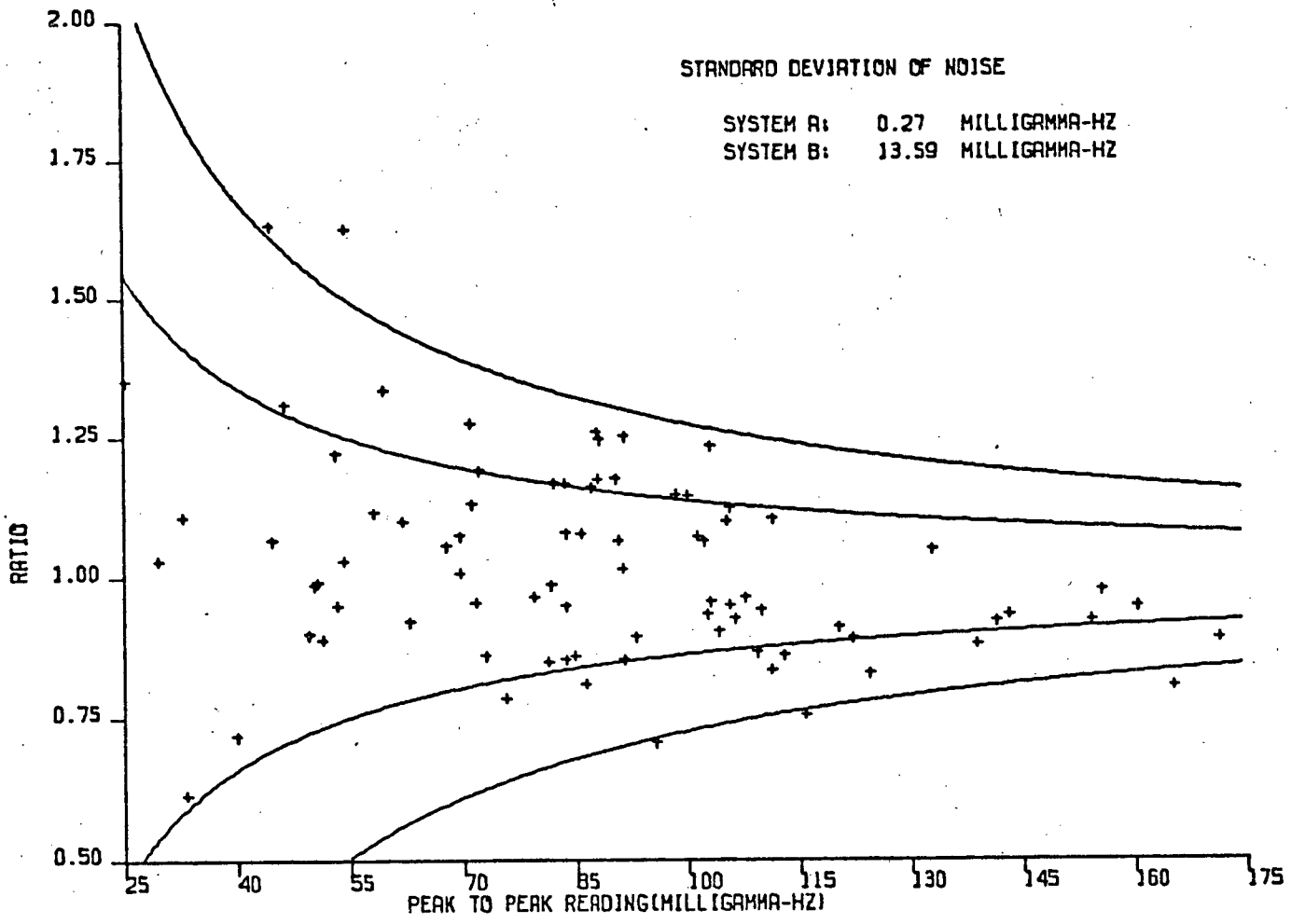

Fig. 4.4. Ratio of system B output to system A output. Ratio is plotted versus system A output. The inside pair of distribution limits correspond to one standard deviation, 68.3%. The outside ones are twice the standard deviation, 95.5%.

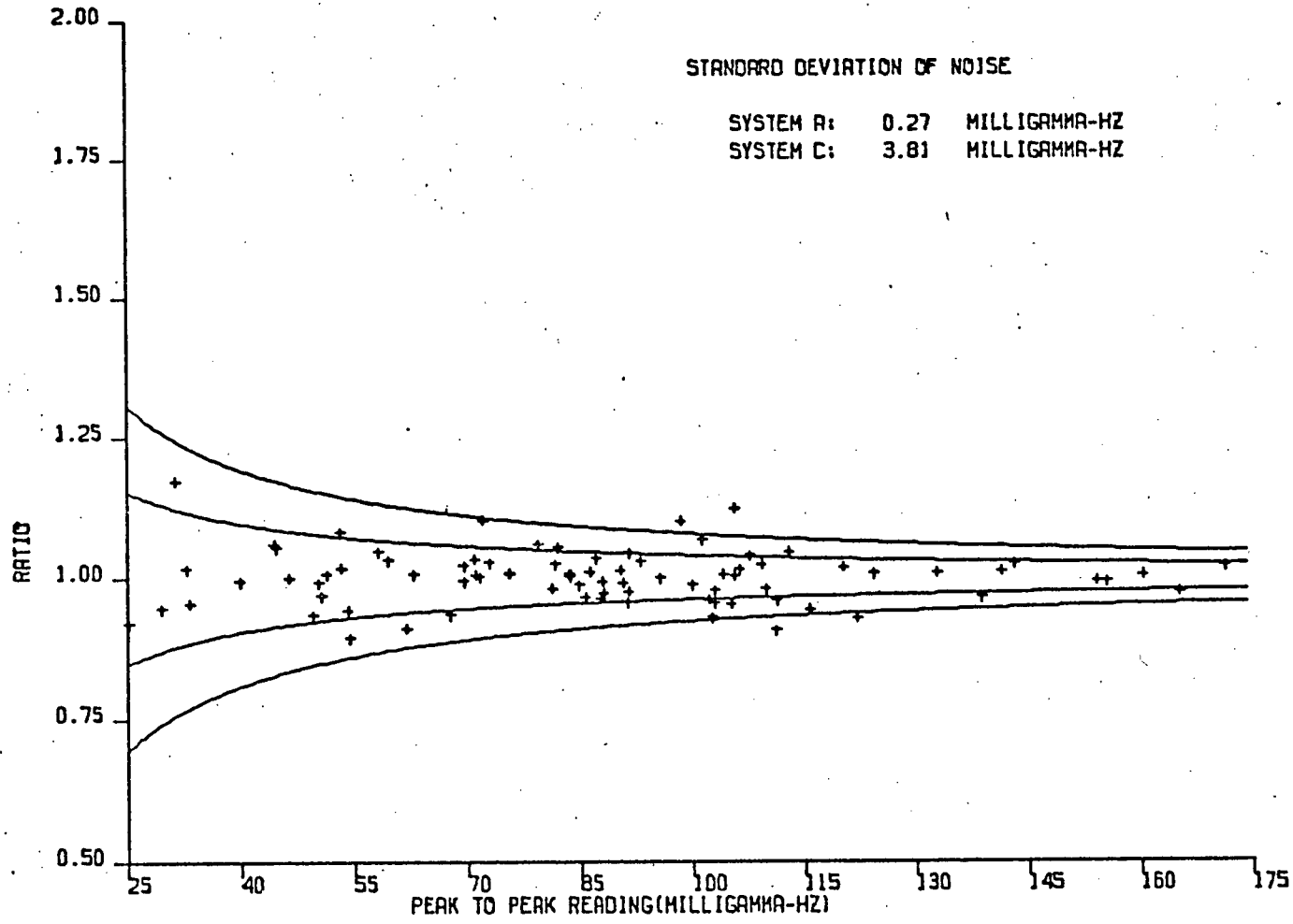

Fig. 4.5. Ratio of system C output to system A output. Ratio is plotted versus system A cutput. The inside pair of distribution limits correspond to one standard deviation, 68.3%. The outside ones are twice the standard deviation, 95.5%.

noise on each channel follows a normal distribution.

4.2.2 NOISE ANALYSIS ON PROBABILITY GRAPH

As defined by the left hand side of the equation 4.2.1-9, differences between the corresponding peak-to-peak readings on the two channels are taken and plotted on a probability graph. The probability, y, that a difference be less than x is given as follows.

$$y = \frac{1}{\sqrt{2\pi}\,\sigma} \int_{-\infty}^{x} e^{-\frac{(x-m)^2}{2\sigma^2}}\, dx \qquad (4.2.2\text{-}1)$$

Providing that the differences form a sample ensemble of normal distribution with mean, m, and a standard deviation, σ ; that is, $N(m,\sigma^2)$. The probability, y, is rewritten as follows.

$$y = \frac{1}{\sqrt{2\pi}} \int_{-\infty}^{t} e^{-\frac{t^2}{2}}\, dt$$

where

$$t = (x-m)/\sigma \qquad (4.2.2\text{-}2)$$

The range of sample values x, is divided into regular intervals of classes, and the cumulative probability, yi, is obtained on each class. For a large number of samples, the cumulative probability should be close to that of a normal distribution.

$$y_i = \frac{1}{\sqrt{2\pi}} \int_{-\infty}^{t_i} e^{-\frac{t_i^2}{2}}\, dt_i \qquad (4.2.2\text{-}3)$$

As the probabilities, yi's, are plotted along the axis of t where t is related to x linearly;

$$t_i = (x_i - m)/\sigma \qquad (4.2.2\text{-}4)$$

The plots should be a straight line if the sample ensemble follows a normal distribution. The reading at t=0 or y=0.5

gives the mean gives the mean value, m. The standard deviation is obtained by the following relation,

$$t_i - t_j = (x_i - x_j)/\sigma \qquad (4.2.2\text{-}5)$$

or

$$\sigma = (x_i - x_j)/(t_i - t_j) \qquad (4.2.2\text{-}6)$$

The standard deviation of noise for comparison between system A and system B is found to be 13.59 milligamma-Hz from Fig . 4.6. In the case of comparison between system A and C, it is found to be 3.81 milligamma-Hz as shown in Fig. 4.7.

4.2.3. PROBABILITY DENSITY FUNCTION OF A RATIO OF TWO NORMAL VARIABLES

The probability density function for the ratio of two normal variables was obtained, for example, by Geary (1935).

Let a and b be constant and also y and x be random variables which follow normal distributions with zero mean and standard deviations β and α , respectively. The ratio value becomes

$$z = \frac{b+y}{a+x} \qquad (4.2.3\text{-}1)$$

if x and y are independent of each other, the joint prcbability, or the probability of simultaneous occurrence of x and y, is given by

$$h(x,y)dxdy = \frac{1}{2\pi\alpha\beta}\, e^{-\frac{1}{2}\left(\frac{x^2}{\alpha^2}+\frac{y^2}{\beta^2}\right)} dxdy \qquad (4.2.3\text{-}2)$$

Changing the variables (x,y) to (x,z) by 4.2.3-1, we get

$$h(x,z)dxdz = h(x,y)\left|\frac{\partial(x,y)}{\partial(x,z)}\right| dxdz$$

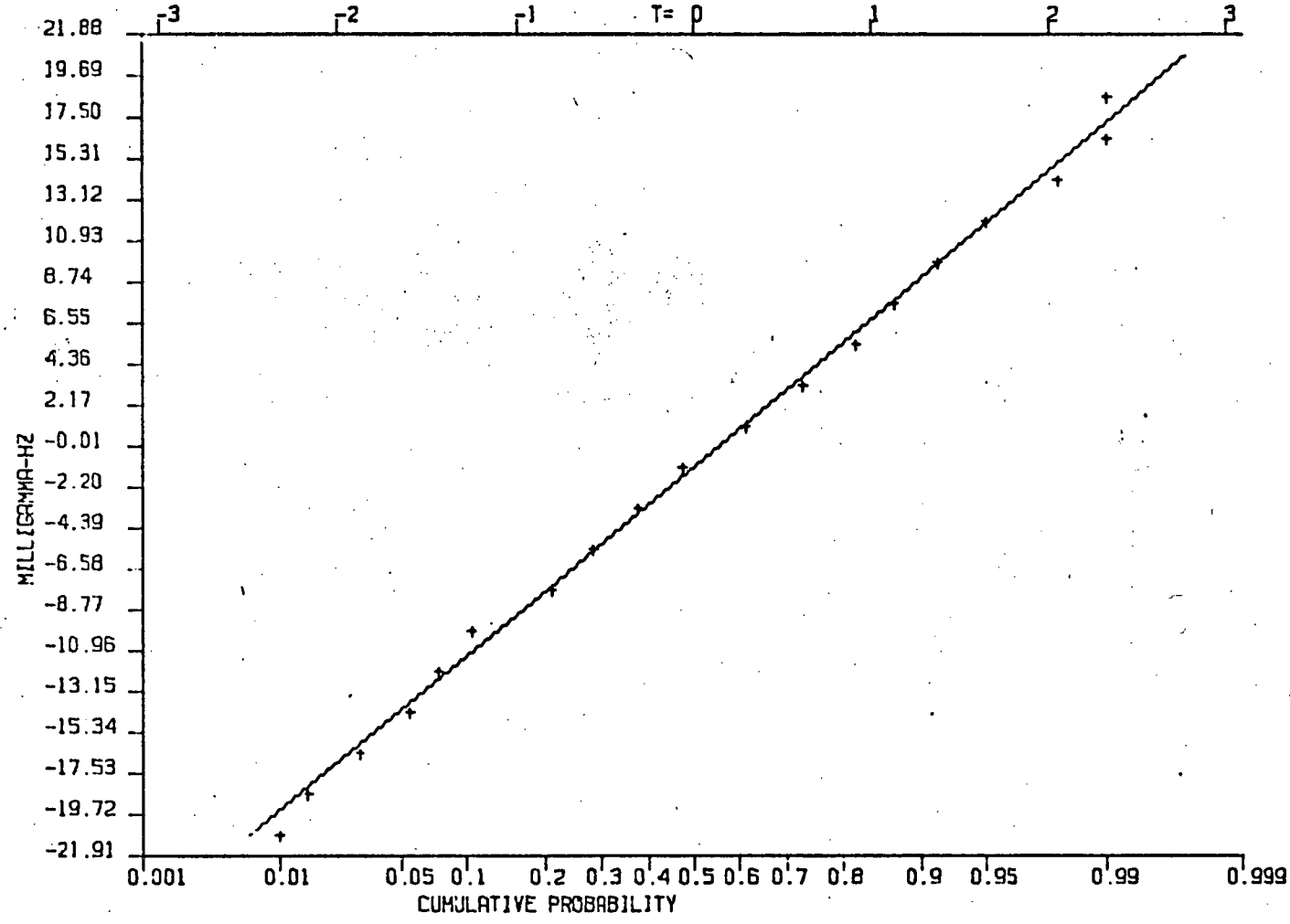

Fig. 4.6. Normal distribution of the difference between signals of system A and B. Mean value is found at t=0. Standard deviation appears as the slope of the line.

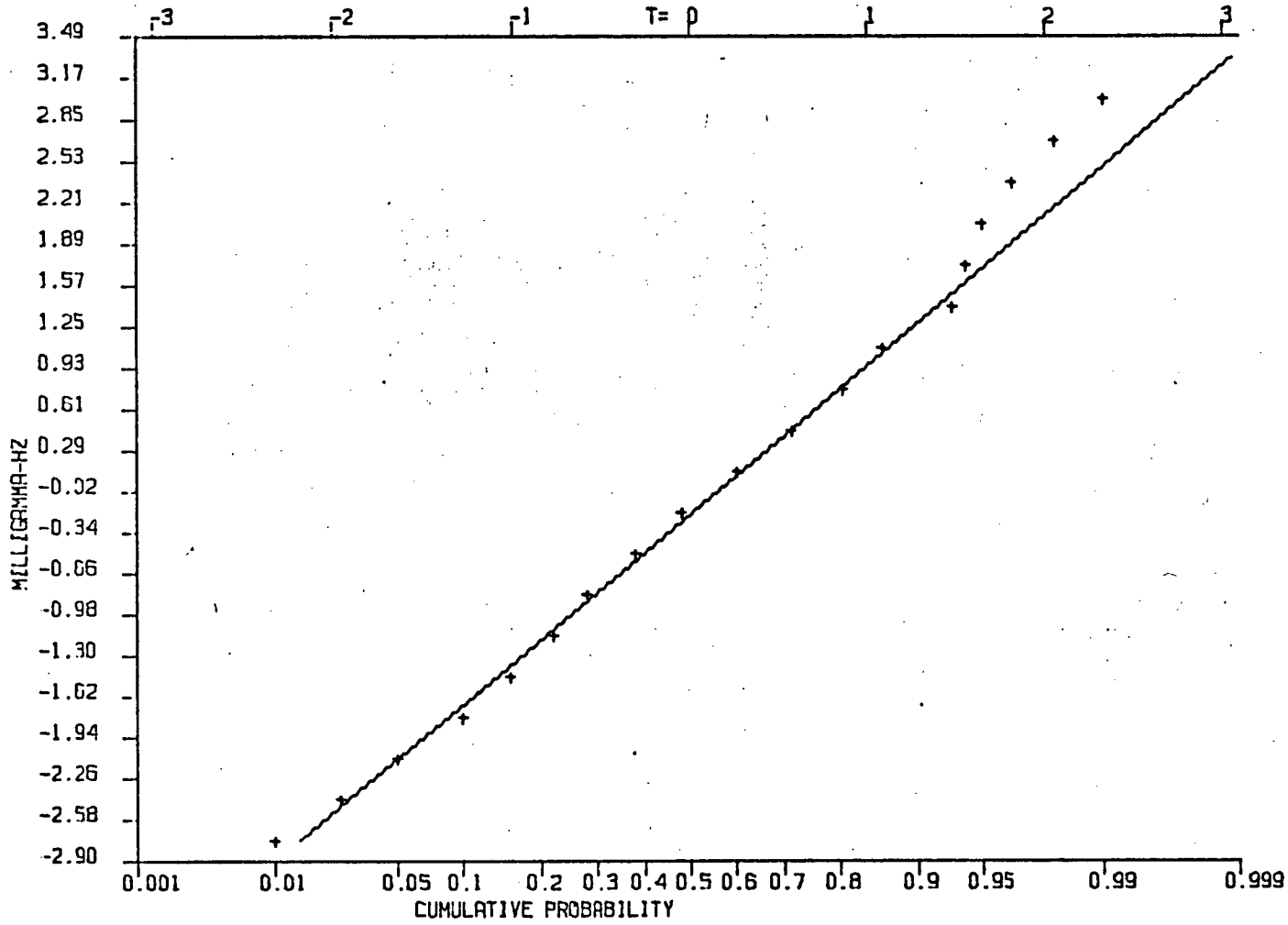

Fig. 4.7. Normal distribution of the difference between signals of system A and C. Mean value is found at t=0. Standard deviation appears as the slope of the line.

$$= \frac{|a+x|}{2\pi\alpha\beta} e^{-\frac{1}{2}\left(\frac{x^2}{\alpha^2}+\frac{y^2}{\beta^2}\right)} dx\,dz \qquad (4.2.3\text{-}3)$$

with $y=(a+x)z-b$ and where $|a+x|$ is a positive value. The probability function P(z) becomes

$$P(z)=\int_{-\infty}^{\infty} h(x,z)dx=\int_{-\infty}^{\infty} g(x,z)dx-2\int_{-\infty}^{-a} g(x,z)dx$$

where

$$g(x,z)=\frac{a+x}{2\pi\alpha\beta} e^{-\frac{1}{2}\left(\frac{x^2}{\alpha^2}+\frac{y^2}{\beta^2}\right)} \qquad (4.2.3\text{-}4)$$

with $y=(a+x)z-b$. Let Q(z) and R(z) represent the first and second integrals on the right hand side of this equation.

$$P(z)=Q(z)+R(z) \qquad (4.2.3\text{-}5)$$

The integration in Q(z) can be performed through a transform of x to x',

$$x'=x+\frac{(az-b)z\alpha^2}{\beta^2+\alpha^2z^2}=x+c \qquad (4.2.3\text{-}6)$$

so that

$$Q(z)=\frac{1}{2\pi\alpha\beta}\int_{-\infty}^{\infty}(a-c+x')e^{-\frac{1}{2}(x'^2+d)}dx \qquad (4.2.3\text{-}7)$$

where $d=\frac{(az-b)^2}{\beta^2+\alpha^2z^2}\{\alpha^2z^2(\alpha^2-1)+\beta^2\}$

Then

$$Q(z)=\frac{1}{\sqrt{2\pi}}\frac{a\beta^2+b\alpha^2z^2}{(\beta^2+\alpha^2z^2)^{3/2}}\exp\left\{-\frac{az-b}{\sqrt{\beta^2+\alpha^2z^2}}\right\} \qquad (4.2.3\text{-}8)$$

Q(z) becomes a normal distribution function by the transform of the variable

$$Q(t)=\frac{1}{\sqrt{2\pi}}e^{-\frac{t^2}{2}}, \quad t=\frac{az-b}{\sqrt{\beta^2+\alpha^2z^2}} \qquad (4.2.3\text{-}9)$$

Practically, Q(z) becomes a good approximation of the probability density function, P(z). From 4.2.3-5,

$$\int_{-\infty}^{\infty} P(z)dz = \int_{-\infty}^{\infty} Q(z)dz + \int_{-\infty}^{\infty} R(z)dz \qquad (4.2.3\text{-}10)$$

The left hand side of the equation is unity.

$$1 = 1 - \epsilon + \int_{-\infty}^{\infty} R(z)dz \qquad (4.2.3\text{-}11)$$

That is the error, ϵ, by equating Q(z) to P(z) is

$$\epsilon = \int_{-\infty}^{\infty} R(z)dz \qquad (4.2.3\text{-}12)$$

In other words, ϵ, is the probability of finding a deviation from the average in absolute value greater than or equal to a/α. It will be noted that $\epsilon/2$ is the probability of finding a negative value of a+x. Since R(z) is a positive function of z, it follows that

$$\int_{z_1}^{z_2} R(z)dz \leq \epsilon \qquad (4.2.3\text{-}13)$$

for all values of z1 and z2. If P(z) denotes the probability of finding a value of z between z1 and z2, it follows from the equation 4.2.3-10 that

$$\int_{z_1}^{z_2} Q(z)dz = Q(z_1, z_2) < P(z_1, z_2) \leq Q(z_1, z_2) + \epsilon \qquad (4.2.3\text{-}14)$$

Even if α/a, the coefficient of variation of a+x, is not greater than 1/3, ϵ is very minute and P(z1,z2) can be taken as equal to Q(z1,z2). In the particular case of $\alpha/a = 1/3$, $\epsilon = 0.0027$.

The expression 4.2.3-8 shows that the variable, t, is normally distributed with zero mean and unit variance. Therefore, $|t| < 1$ gives the range of 68.3% for the ratio value

distribution. $|t|<2$ gives the range of 95.5%. To draw these distribution limits, the results of 4.2.1 are used together with the standard deviation of noise of system A which is estimated from records of geomagnetically quiet days. It is 0.27 milligamma-Hz.

4.3. EFFECTIVE PERMEABILITY OF PERMALLOY CORE

In the section 4.2.1 relative sensitivities of the permalloy core coil systems with respect to the air core coil system were obtained. With these values, the effective permeability of each of the permalloy cores is calculated as follows.

From section 3.2, output of the air core coil system will be 0.0235 volts per sinusoidal geomagnetic variations of 1 milligamma-Hz. Then, output of a permalloy core coil system with relative sensitivity, S, is 0.0235xS volts. Knowing the total gain of the amplifier of this system, G, we get an estimate of the output voltage of the sensor coil as

$$Vc = 0.0235 S/A$$

The relation 3.2-6 gives the effective permeability such as

$$\bar{\mu}_e = \left(\frac{1}{2\pi}\right)\frac{Vc}{NA}\cdot 10^{-12}$$

The constants given in Table 3.1 are used. The effective permeability of system B is obtained as 152 while that of system C as 146.

According to Fig. 2.1, the apparent permeability is expected to be 800 for the core whose length to diameter ratio is 50. The apparent permeability of 150 can be obtained when true permeability is 150, but this value is extraordinarily

small for a ferromagnetic material such as permalloy. Besides, this low apparent permeability is in the nonlinear region where sensor response depends more on the permeability of the core. It is possible in this case that the dynamic response for a biased fluctuation of the earth's magnetic field is subjected to much smaller permeability, namely the incremental permeability (Bozorth,1951). Its response may appear linear within a small amplitude of magnetic field fluctuation.

4.4 COMPARISON OF POWER SPECTRA

The records by the three systems, 282 sec long duration starting at 21h 42m 06s UT on October 10, 1973, were taken and their power spectra were obtained for another interchannel comparison.

The conventional Blackman-Tukey method as well as the maximum likelihood method were employed for estimating the power spectrum of each. The maximum likelihood power estimator is taken first with an intention of obtaining a reference for the Blackman-Tukey method because it is excellent for reproducing spectral estimators out of relatively small number of data points (Lacoss 1971). A derivation of the maximum likelihood power estimate is given in the appendix. Various lengths of autocorrelation were tried with the Blackman-Tukey method until its spectral estimate becomes closest to the one given by the maximum likelihood method. Then a confidence interval for the spectral estimator as well as the bandwidth was calculated from the window shape and the length of the autocorrelation used.

4.4.1. CONFIDENCE INTERVAL AND BANDWIDTH OF THE TUKEY WINDOW

According to the Blackman-Tukey method, power spectra are estimated by taking the Fourier transform of the autocorrelation. This autocorrelation is calculated directly from a sampled length of time series data and then it is truncated and/or weighted with a window function. The Tukey window, or cosine bell, used here for weighting the autocorrelation is given in lag window form as

$$w(u)\begin{cases}\frac{1}{2}(1+\cos\frac{\pi u}{M}) & \text{for } |u|\leq M\\ 0 & \text{for } |u|>M\end{cases} \qquad (4.4.1\text{-}1)$$

where M is the length of the truncated autocorrelation. Sthis weighting is equivalent to smoothing the raw spectra, which is a direct Fourier transform of data of time domain, through a bandpass filter. The bandwidth of this spectral window, b, is defined as

$$\frac{1}{b}=\int_{-\infty}^{\infty} w^2(u)\,du = M\int_{-1}^{1} w^2(v)\,dv = M K_w \qquad (4.4.1\text{-}2)$$

where $u = Mv$, and

$$K_w=\int_{-1}^{1} w^2(v)\,dv=\int_{-1}^{1}\frac{1}{4}(1+\cos\pi v)^2\,dv=0.75 \qquad (4.4.2\text{-}3)$$

That is, the bandwidth is related to M by

$$b=(0.75M)^{-1} \qquad (4.4.1\text{-}4)$$

The smoothed sample spectra C(f) estimated thrcugh the above windowing is

$$E[\bar{C}(f)]=\int_{-T}^{T} w(u)R(u)e^{-i2\pi fu}\,du \qquad (4.4.1\text{-}5)$$

where R(u) is the autocorrelation and T is the length of the

time series data. In the frequency domain,

$$E[\bar{C}(f)]=\int_{-\infty}^{\infty} M W(g)\, P(f-g)\, dg \qquad (4.4.1\text{-}6)$$

where

$$W(f)=\int_{-\infty}^{\infty} w(u)\, e^{i2\pi fu}\, du \qquad (4.4.1\text{-}7)$$

If P(f) varies smoothly relative to the bandwidth, b, then

$$E[\bar{C}(f)]=P(f)\int_{-\infty}^{\infty} W(g)\, dg \simeq P(f) \qquad (4.4.1\text{-}8)$$

Using Parseval's theorem, the variance of smoothed spectral estimator may be described.

$$Var[\bar{C}(f)]\simeq \frac{P^2(f)}{T}\int_{-\infty}^{\infty} w^2(u)\, du = P^2(f)\frac{I}{T} \qquad (4.4.1\text{-}9)$$

That is,

$$I=\int_{-\infty}^{\infty} w^2(u)\, du = 1/b \qquad (4.4.1\text{-}10)$$

With this mean and variance, $\bar{C}(f)$ can be approximated to random variable, $a\chi^2$, which follows chi-squared distribution with degrees of freedom, ν.

$$\nu = 2\{E[\bar{C}(f)]/Var[\bar{C}(f)]\} \qquad (4.4.1\text{-}11)$$

$$a \simeq E[\bar{C}(f)]/\nu \qquad (4.4.1\text{-}12)$$

In other words, the random variable, $\nu\bar{C}(f)/P(f)$, is distributed as a χ^2 with degrees of freedom, ν. To find the $100(1-\alpha)\%$ distribution range of $\nu\bar{C}(f)/P(f)$, we refer to the table of chi-square distribution which gives $\chi_\nu(1-\frac{\alpha}{2})$ and $\chi_\nu(\frac{\alpha}{2})$ in the relation,

$$Pr\{\chi_\nu(\tfrac{\alpha}{2}) < \frac{\nu\bar{C}(f)}{P(f)} \leq \chi_\nu(1-\tfrac{\alpha}{2})\} = 1-\alpha \qquad (4.4.1\text{-}13)$$

where $Pr\{\chi^2 < \chi_\nu(\frac{\alpha}{2})\} = \frac{\alpha}{2}$

Then confidence interval for P(f) becomes

$$\frac{\nu \bar{C}(f)}{\chi_\nu(1-\frac{\alpha}{2})} \leq P(f) < \frac{\nu \bar{C}(f)}{\chi_\nu(\frac{\alpha}{2})} \qquad (4.4.1\text{-}14)$$

In logarithmic scale,

$$\log \bar{C}(f) + \log \frac{\nu}{\chi_\nu(1-\frac{\alpha}{2})} \leq \log P(f) < \log \bar{C}(f) + \log \frac{\nu}{\chi_\nu(\frac{\alpha}{2})} \qquad (4.4.1\text{-}15)$$

Therefore, from the value of $\log \bar{C}(f)$, $\log \nu/\chi_\nu(1-\frac{\alpha}{2})$ is the lower limit and $\log \nu/\chi_\nu(\frac{\alpha}{2})$ is the higher limit of the interval in which the true value of the spectrum P(f), cculd fall with probability, $100(1-\alpha)$%. These limits depend only on the confidence and the degrees of freedom which are related to M by

$$\nu = \frac{2T}{I} = 2Tb = T/0{,}35M \qquad (4.4.1\text{-}16)$$

Therefore M controls the bandwidth and confidence level at the same time.

4.4.2. RESULTS OF SPECTRAL ANALYSIS

Table 4.2 show the numerical results of spectral analysis. Spectrum patterns are given on Fig. 4.8, Fig. 4.9 and Fig. 4.10.

These spectrum peaks occur in a position corresponding well to the ones obtained by the maximum likelihood methcd. Three peaks at 0.110Hz, 0.138Hz and 0.166Hz seem to be noise because of their low level, lower than -20db, with respect tc the main peak. The difference in power spectrum between the air core coil system and each of the permalloy core coil systems is well within 96% confidence intervals.

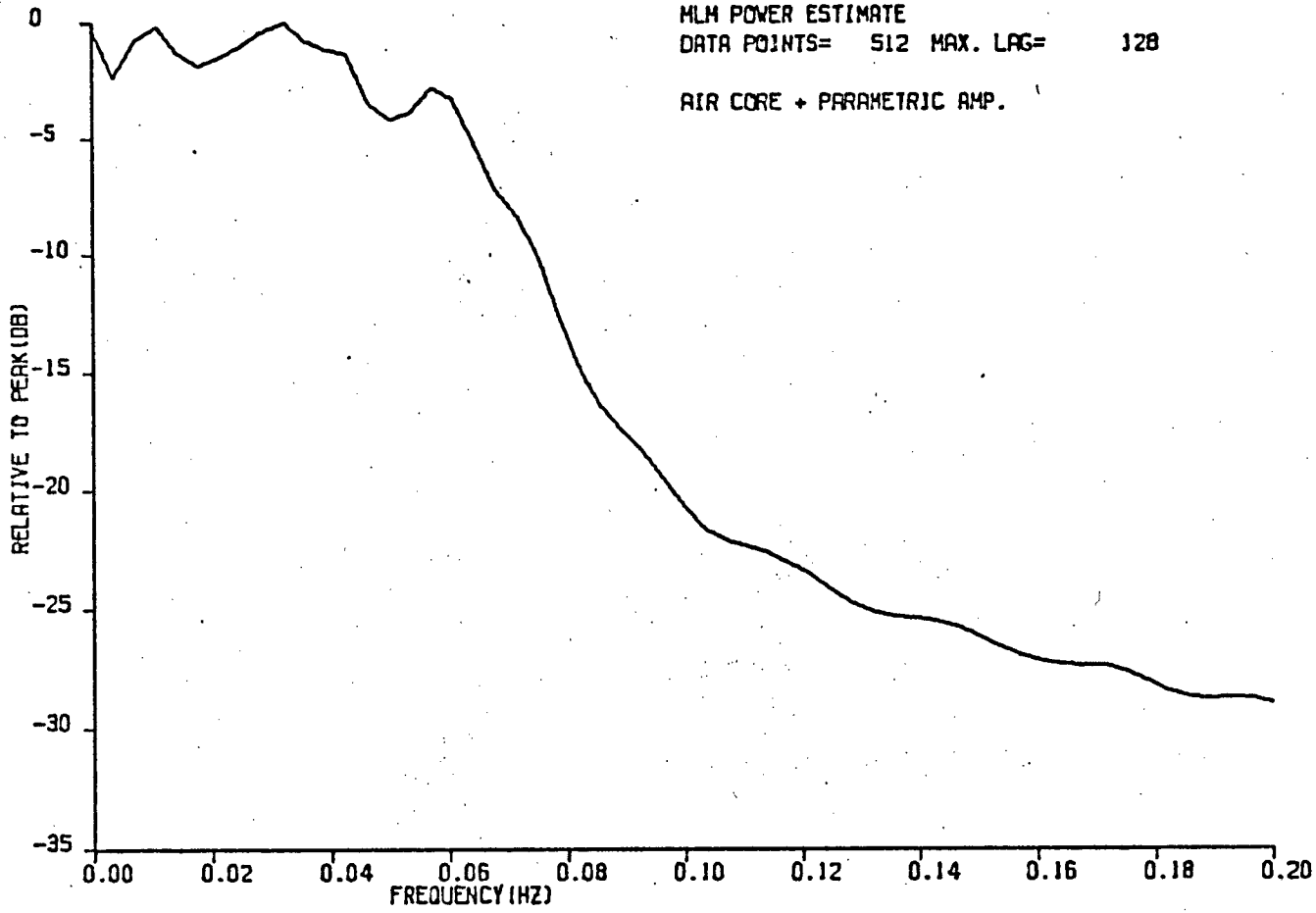

Fig. 4.8. Maximum likelihood power estimate of system A record of October 10, 1973. (see Fig. 4.1.)

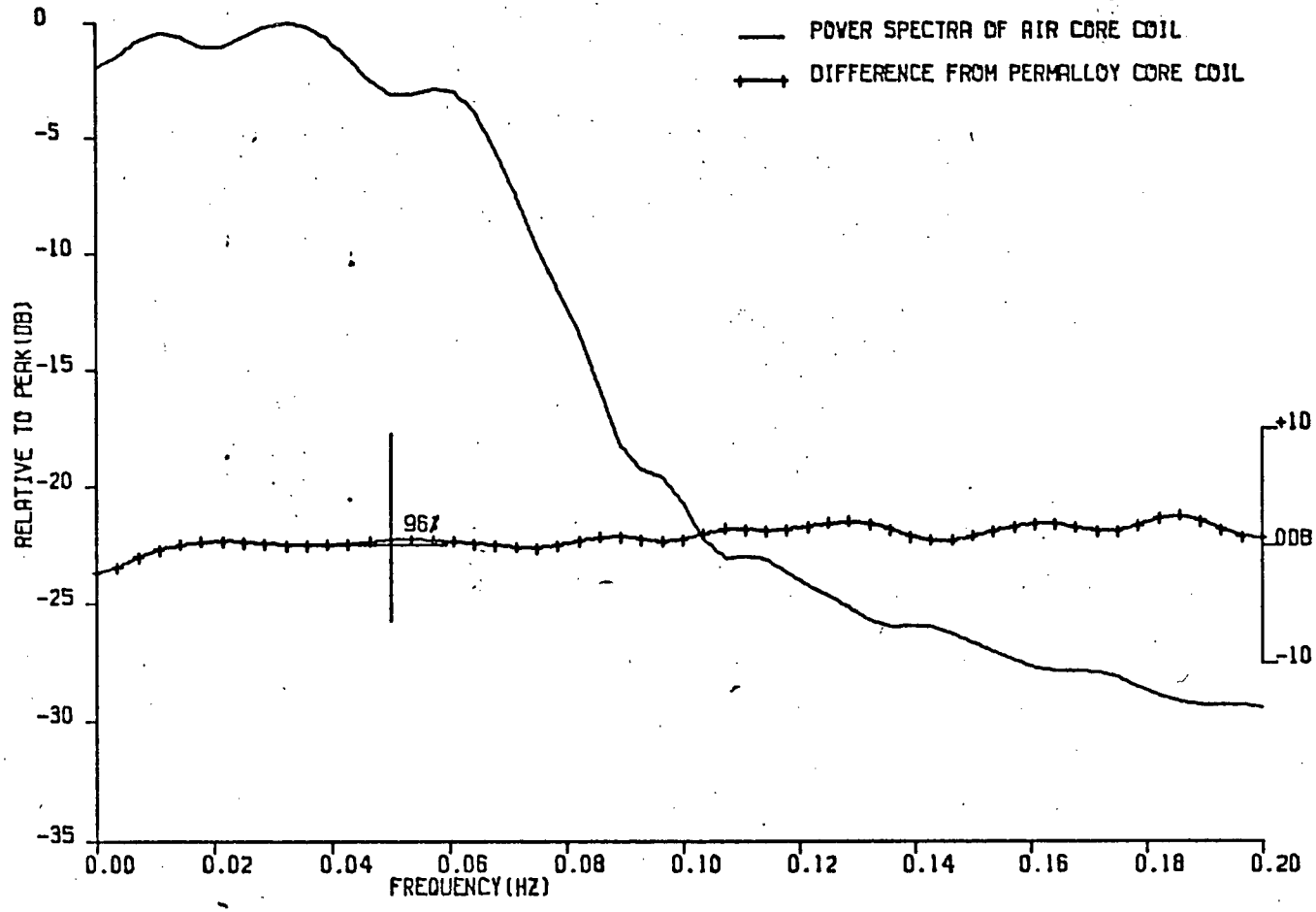

Fig. 4.9. Difference in power spectra of system B record by Blackman-Tukey method. The horizontal cross line shows the bandwidth, and the vertical one is the 96% confidence interval. Also, the center point corresponds to zero difference of power spectra by the scale on the right hand side. Difference of power spectra is taken after each spectrum is normalized to its peak.

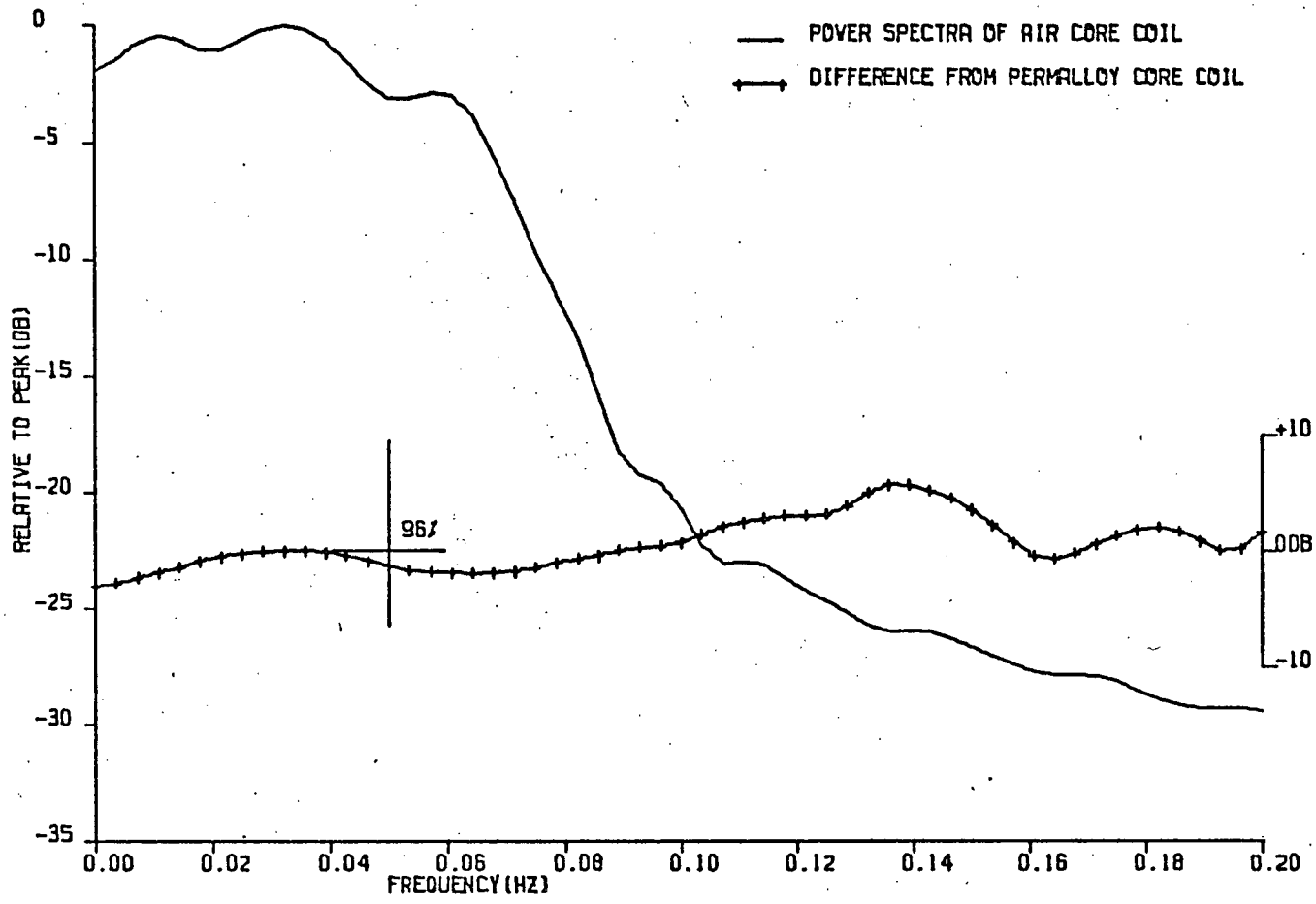

Fig. 4.10. Difference in power spectra of system C record by Blackman-Tukey method. The horizontal cross line shows the bandwidth, and the vertical one is the 96% confidence interval. Also, the center pcint corresponds to zero difference of power spectra by the scale on the right hand side. Difference of pcwer spectra is taken after each spectrum is normalized to its peak.

Peaks in the power spectrum of the air core coil signal				Difference from Permalloy core coil signal	
Maximum likelihood		Blackman-Tukey		System B	System C
Hz	db	Hz	db	db	db
0.0106	-0.2053	0.0106	-0.4235	-0.9582	-0.2095
0.0318	0.0*	0.0318	0.0*	0.0*	0.0*
0.0566	-2.7992	0.0566	-2.856	-0.9299	0.1953
-	-	0.110	-22.9825	1.2436	0.6705
-	-	0.138	-25.9197	2.2864	0.3714
-	-	0.166	-27.8723	-0.0956	0.7654
0.191	-28.697	0.191	-29.3180	0.0206	0.6641

Table 4.2. Comparison of power spectra. Each spectra are normalized to its peak. That is, peaks with '*' are arbitrarily set to 0.0db.

5. SUMMARY AND CONCLUDING REMARKS

In the region of high to mid geomagnetic latitude, correlations between geomagnetic micropulsation data obtained at various stations provide important information. For example, with the data along the geomagnetic meridian it is interesting to study the behavior of the plasma pause as well as the electro magnetic phenomena associated with this boundary. The induction magnetometer covers the entire frequency band of the micropulsation signal. For the field observation, a ferromagnetic iron core coil is a practical choice of sensor because of its physical constants. But, contrary to theories about the large open loop coil, or air core coil, the role of the ferromagnetic core is not free from speculatiens.

Three geomagnetic micropulsation detection/recording systems, one using an air core coil sensor and the other two permalloy core coil sensors, have been run simultaneously since September 20, 1973. The analysis carried on the data of October 10, 1973 reveals that the permalloy core coil sensors produce no significant distortion in the output signals compared to the air core coil system. The permalloy core coil sensors were designed to be portable whereas the air core coil was designed for use at a permanent station. The ratio of two signals, or more specifically, a peak-to-peak reading by each of the permalloy core coil systems divided by the corresponding value of the air core coil system, was found to fall in the vicinity cf the value 1. The plots are more scattered as the S/N becomes poorer, but it is still within the predicted limits based on an estimation of noise. The power spectrum was estimated for each of the

three by Blackman-Tukey method as well as the maximum likelihood method. No significant difference was recognized among these spectra.

The explanation for these results may be that the nonlinear response inherent to any ferromagnetic material is suppressed by the demagnetization effect. The theory of the demagnetization effect also suggests that a ferromagnetic core coil is more sensitive if it is longer. As the core becomes longer, permeability of the core material is required tc be higher to suppress the nonlinear response.

Although, the emphasis is placed on the demagnetization effect, other effects of ferromagnetism should be taken into account for the interpretation of the actual core response. The incremental permeability, for example, seems to explain considerable reduction of the effective permeability of the core (see appendix 2). Also, further analyses should be done on the records of better quality, especially better S/N.

APPENDICES

1. MAXIMUM LIKELIHOOD POWER ESTIMATOR

The Blackman-Tukey method of power estimation is a procedure which infers from a finite length of data a better approximation of the autocorrelation calculated for an infinite data. The weight function, which is applied to the autocorrelation, is rather artificial.

The maximum likelihood is based on a different concept. The power estimation process is designed to pass the signal through but to attenuate and minimize the residual power at the output. Because this minimizing, or optimization of the process, is done for individual power estimator, it is regarded as a data adaptive method.

An electrical analog of this process is a filter. Based on the above concept, this filter is designed as follows. For an input which consists of signal and zero mean noise produced by a random process.

$$x_k = A e^{i2\pi f \Delta k} + n_k \tag{A-1}$$

where k is a time index and Δ is the sampling interval. Output of this filter retains the signal.

$$y_k = \sum_{n=1}^{N} h_n x_{k+1-n} = A e^{i2\pi f \Delta k} \tag{A-2}$$

With A-1, this is reduced to

$$1 = \sum_{n=1}^{N} h_n e^{i2\pi f (1-n)\Delta} \tag{A-3}$$

In matrix notation, column vectors are defined as follows.

$$\underline{a} = col(h_1, h_2, \cdots, h_n) \tag{A-4}$$

$$E = col(1, e^{i2\pi f\Delta}, \cdots, e^{i2\pi f(N-1)\Delta}) \tag{A-5}$$

A-3 becomes

$$1 = E^{*T}\underline{a} \tag{A-6}$$

The other condition is that the variance of the noise is to be minimized.

The variance of output, y, is

$$\sigma^2 = \langle (y_k - \langle y_k \rangle)^2 \rangle \tag{A-7}$$

$$= \langle y_k^2 \rangle \tag{A-8}$$

$$= \langle \{ A e^{i2\pi f\Delta k} + \sum_{l=1}^{N} a_l n_{k+1-l} \}^2 \rangle \tag{A-9}$$

$$= \langle \{ \sum_{l=1}^{N} a_l n_{k+1-l} \}^2 \rangle \tag{A-10}$$

$$= \langle \{ \sum_{l=1}^{N} h_l n_{k+1-l} \}^2 \rangle \tag{A-11}$$

$$= \langle \{ \sum_{l=1}^{N} h_l n_{k+1-l} \} \{ \sum_{m=1}^{N} h_m^* n_{k+1-m} \} \rangle \tag{A-12}$$

The correlation is defined as

$$\rho_{lm} = \langle n_{k+1-l}\, n_{k+1-m} \rangle \tag{A-13}$$

A-10 becomes

$$\sigma^2 = \langle h_k \rho_{lm} h_k^* \rangle \tag{A-14}$$

$$= \underline{a}^T R \underline{a}^* \tag{A-15}$$

where R is N by N correlation matrix.

A-13 is to be minimized under the constraint A-4. Taking Lagrange's multiplier method, we first rewrite A-4.

$$g = E^{*T}\underline{a} - 1 = 0 \tag{A-16}$$

Then, with $a_l = \alpha_l + i\beta_l$

$$\frac{\partial \sigma^2}{\partial \alpha_l} = \theta \frac{\partial g}{\partial \alpha_l}, \qquad \frac{\partial \sigma^2}{\partial \beta_l} = \theta \frac{\partial g}{\partial \beta_l} \tag{A-17}$$

where θ is an undetermined multiplier.

Or
$$2\rho_{em}\alpha_\ell = \theta \exp\{-i2\pi f \Delta \ell\}$$
$$2\rho_{em}\beta_\ell = \theta \exp\{-i2\pi f \Delta \ell\} \qquad \text{(A-18)}$$

In matrix notation,
$$R\underline{a} = \frac{\theta}{2}E^* \qquad \text{(A-19)}$$

The filter coefficient vector becomes
$$\underline{a} = \frac{\theta}{2}R^{-1}E^* \qquad \text{(A-20)}$$

This is substituted into a complementary equation to A-4,
$$1 = E^*\underline{a} \qquad \text{(A-21)}$$

which describes the negative frequency region. So that,
$$1 = E^T\frac{\theta}{2}R^{-1}E^* \qquad \text{(A-22)}$$

Eliminating θ with A-17, we get
$$\underline{a} = \frac{R^TE^*}{E^TR^{-1}E^*} \qquad \text{(A-23)}$$

The power estimator by the maximum likelihood method is
$$P_L = \langle y_k^2 \rangle = \sigma^2 \qquad \text{(A-24)}$$

Finally,
$$P_L = \underline{a}^{*T}R\,\underline{a} = \frac{1}{E^TR^{-1}E^*} \qquad \text{(A-25)}$$

2. INCREMENTAL PERMEABILITY

The ordinary hysteresis curve describes the monotonically increasing or decreasisng magnetization, or DC magnetization between the saturation limits. The hysteresis response also occurs when magnetic field consists of an alternating field and a relatively large bias field. Bozorth(1951) reviewd this phenomena.

In the presense of a relatively large bias field, the

alternating field produces magnetic induction which follows minor hystersis loops bounded to the major loop at one of its tips. In most cases the slope of each branch of these subloops is less steep than the main loop. These are shown in Fig.A-1.

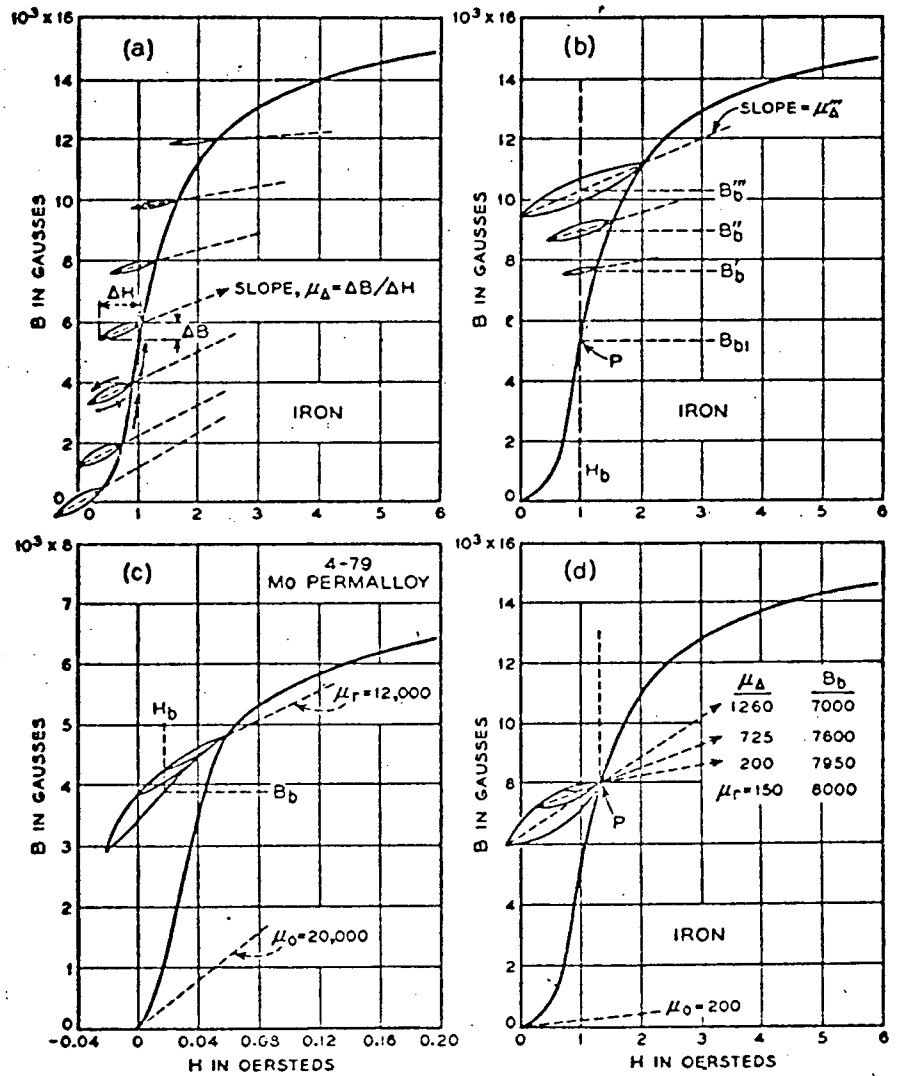

Fig.A-1. Minor hysteresis loops taken under various conditions in iron (a,b,d) and 4-79 Permalloy (c). (from Bozorth 1951)

Briefly, the permeability for the exitation of a variational magnetic field becomes much less than the one traced by DC magnetization. The incremental permeability, μ_i, is defined as the average of each branch. The reversible permeability, μ_r, is the asymptotic value when the amplitude of the alternating

field, H_i', is increased, the incremental permeability is also increased in a linear relation such as $\mu_i' = \mu_r + \nu_i' H_i'$, where $\nu_i' = d\mu_i'/dH_i'$.

Fig.A-2 shows that 45 Permalloy has the initial permeability of 2.4x 10^3. Its nominal permeability by DC magnetization is about 5x 10^3 for a field of 0.5 oersted. The incremental permeability becomes 1x 10^3 at this bias. In the case of pure iron, the difference between the incremental permeability and the one by DC magnetization appears even more pronounced (see Fig.A-1(d)).

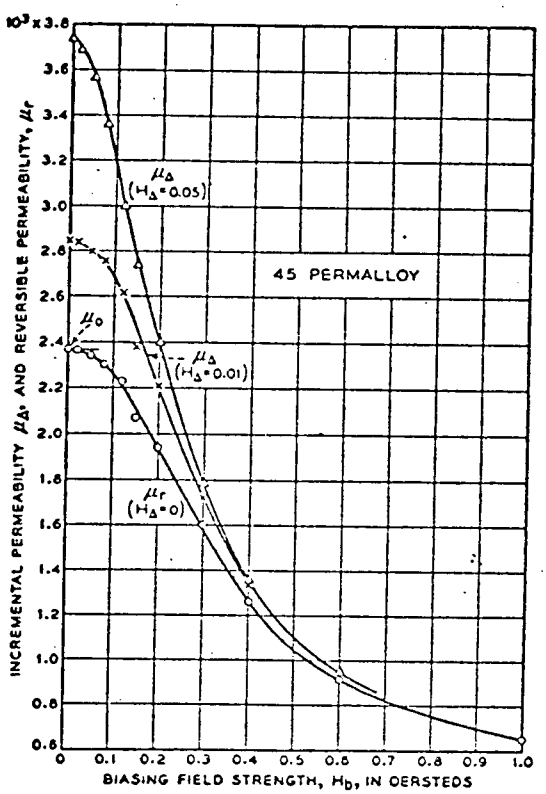

Fig.A-2. Incremental and reversible permeabilities of 45 Permalloy measured with various biasing fields and incremental field strength. (from Bozorth 1951)

It was suggested by Gans(1910) that the reversible permeability is determined by the bias induction, B_b. The

departure from this simplification is not large in case of some materials. Fig.A-3 shows the plot for 45 Permalloy.

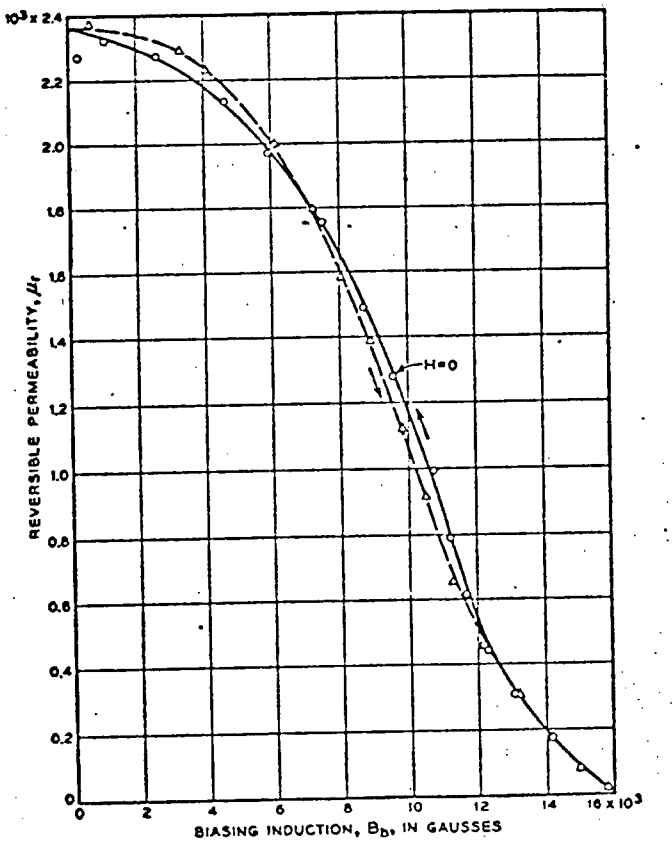

Fig.A-2. Reversible permeability vs induction for 45 Permalloy. (form Bozorth 1951)

But, genarally, there are wide differences in the reversible permeability curves for different materials. Four different characteristics are shown in Fig.A-4.

The reversible permeability is a measure of the firmness with which the magnetic domains are held in position by the biasing field. The magnetic domain is discussed by models which depend on the composition of the material. These models are: i) the magnetic domain has no principal direction of easy magnetization, ii) the direction of the domains are restricted so that they always lie parallel or antiparallel to the field,

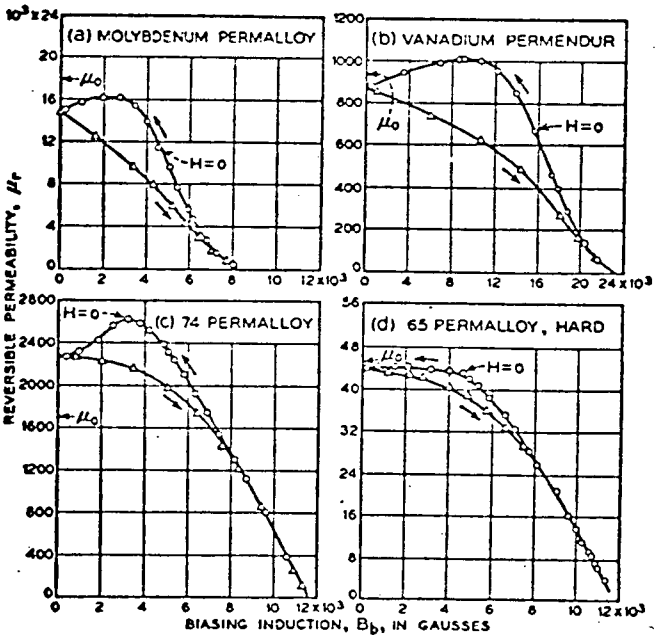

Fig.A-4. Reversible permeability as dependent on biasing induction in (a) Molybdenum Permalloy, (b) Vanadium Permendur, (c) Permalloy containing 74% nickel and (d) hard Permalloy containing 65% nickel. (from Bozorth 1951)

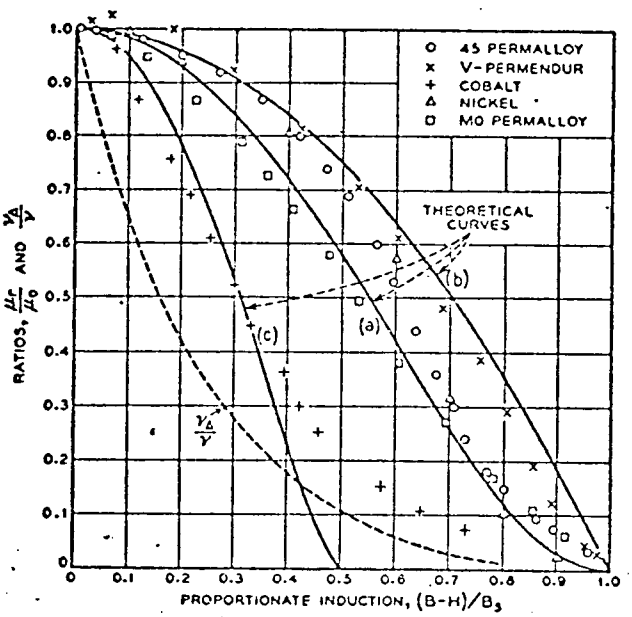

Fig.A-5. Reduced reversible permeability vs reduced biasing induction for several materials, in comparison with the theory: (a) Gans' relation, (b) isotropic domains, (c) anisotropic domains (Brown). Broken curve shows the approximate change in du/dH (for weak fields) as dependent on biasing induction, observed for a variety of materials. (from Bozorth 1951)

iii) they lie parallel or anti parallel to a single crystallographic direction in crystals that are oriented at random in the material. The third model is designed for cobalt by Brown(1938). With these assumptions, the differences in the reversible permeability of different materials are further coincided by plotting μ_r/μ_o against B_b/B_s, where μ_o is the initial permeability and B_s is the induction at saturation, in Fig.A-5.

An interesting case of superposition of field occurs when a weak alternating field is applied at right angles to a constant field. Fig.A-6 shows that the reversible permeability of Molybdenum Permalloy is larger than the ordinary one except at the end points where these values must coincide.

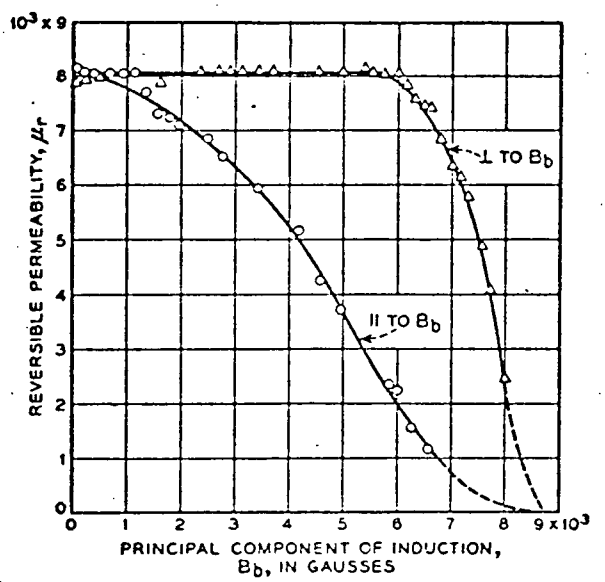

Fig.A-6. Effect of biasing induction on reversible permeability when it is measured parallel or perpendicular to the direction of measurement. (from Bozorth 1951)

REFERENCES

Bozorth, R. M. (1951). Ferromagnetism, New York, Van Nostrand Co., pp.968.

Brown, W. F. (1938). Domain theory of ferromagnetics under stress III. Reversible susceptibility, Physical Review, 54, 279-299.

Campbell, W. H. (1967). Induction loop antennas for geomagnetic field variation measurement, ESSA Technical Report, ERL 123-ESL 6.

Caner, B. (1970). Design considerations, induction coils for micropulsation measurement at Victoria Magnetic Observatory, Unpublished report, Victoria Geophysical Observatory, R. R. 7 Victoria, B. C.

Gans, R. (1910). Magnetic corresponding states, Physkalisch Zeitschrift. 11, 988-991.

Geary, R. C. (1930). The frequency distribution of the quotient of two normal variables, Journal of Royal Statistics Society, 93, 442-444.

Jenkins, G. M. and D. G. Watts, (1968). Spectral Analysis and Its Application, San Francisco, Holden Day Inc., pp.525.

Kollar, F. and R. D. Russell, (1966). Seismometer analysis using an electric current analog, Bulletin of the Seismological Society of America, 56, 1193-1205.

Lacoss, R. T. (1971). Data adaptive spectral analysis methcds, Geophysics, 36, 661-675.

Osborn, J. A. (1945). Demagnetizing factors of the general

ellipsoid, Physical Review, 67, 351-357.

Peterson, E. (1928). Harmonic production in ferromagnetic materials at low frequency and low flux densities, Bell System Technical Journal, 7, 762-796.

Stratton, J. A. (1941). Electromagnetic Theory, New York and London, McGraw-Hill Inc., pp.615.